Nucleic Acids Research, 2024, 1–19
https://doi.org/10.1093/nar/gkae261
Gene regulation, Chromatin and Epigenetics

KDM5-mediated transcriptional activation of ribosomal protein genes alters translation efficiency to regulate mitochondrial metabolism in neurons

Matanel Yheskel[1], Hayden A.M. Hatch[2], Erika Pedrosa[3], Bethany K. Terry[1], Aubrey A. Siebels[2], Xiang Yu Zheng[1], Laura E.R. Blok[4], Michaela Fencková[4,5], Simone Sidoli[6], Annette Schenck[4], Deyou Zheng[1,2,7], Herbert M. Lachman[1,2,3,8] and Julie Secombe[1,2,*,†]

[1]Department of Genetics, Albert Einstein College of Medicine, Bronx, NY 10461, USA
[2]Dominick P. Purpura Department of Neuroscience, Albert Einstein College of Medicine, Bronx, NY 10461, USA
[3]Department of Psychiatry and Behavioral Sciences, Albert Einstein College of Medicine, Bronx, NY 10461, USA
[4]Department of Human Genetics, Donders Institute for Brain, Cognition and Behaviour, Radboud University Medical Center, 6525 Nijmegen, GA, The Netherlands
[5]Department of Molecular Biology and Genetics, Faculty of Science, University of South Bohemia, Ceske Budejovice 370 05, Czechia
[6]Department of Biochemistry, Albert Einstein College of Medicine, Bronx, NY 10461, USA
[7]Department of Neurology, Albert Einstein College of Medicine, 1300 Morris Park Ave., Bronx, NY 10461, USA
[8]Department of Medicine, Albert Einstein College of Medicine, 1300 Morris Park Ave., Bronx, NY 10461, USA

*To whom correspondence should be addressed. Tel: +1 718 430 2698; Email: julie.secombe@einsteinmed.edu
†Lead contact.

Abstract

Genes encoding the KDM5 family of transcriptional regulators are disrupted in individuals with intellectual disability (ID). To understand the link between KDM5 and ID, we characterized five *Drosophila* strains harboring missense alleles analogous to those observed in patients. These alleles disrupted neuroanatomical development, cognition and other behaviors, and displayed a transcriptional signature characterized by the downregulation of many ribosomal protein genes. A similar transcriptional profile was observed in *KDM5C* knockout iPSC-induced human glutamatergic neurons, suggesting an evolutionarily conserved role for KDM5 proteins in regulating this class of gene. In *Drosophila*, reducing KDM5 changed neuronal ribosome composition, lowered the translation efficiency of mRNAs required for mitochondrial function, and altered mitochondrial metabolism. These data highlight the cellular consequences of altered KDM5-regulated transcriptional programs that could contribute to cognitive and behavioral phenotypes. Moreover, they suggest that KDM5 may be part of a broader network of proteins that influence cognition by regulating protein synthesis.

Graphical abstract

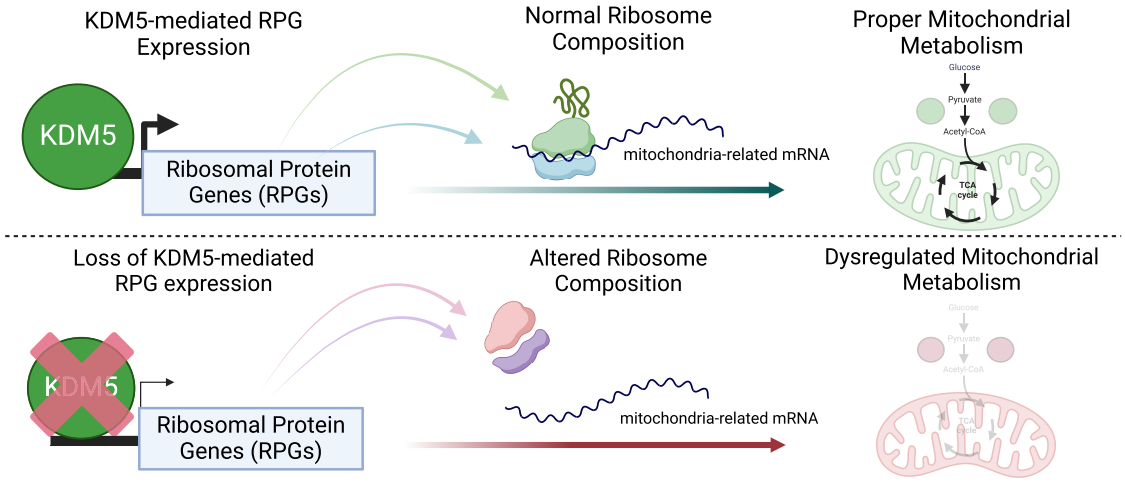

Received: November 9, 2023. **Revised:** March 20, 2024. **Editorial Decision:** March 24, 2024. **Accepted:** March 31, 2024

Introduction

Lysine demethylase 5 (KDM5) family proteins play key roles in the regulation of gene expression programs needed for normal development by binding to, and enzymatically altering, chromatin (1,2). Molecularly, KDM5 proteins can alter transcription by cleaving trimethyl groups from lysine 4 of histone H3 (H3K4me3) to alter promoter activity in addition to demethylase-independent means of gene regulation control. In mammalian cells, three paralogous *KDM5* genes are broadly expressed but appear to be particularly important for brain development and function. This is based on the observation that genetic variants that disrupt *KDM5A*, *KDM5B* or *KDM5C* are associated with intellectual disability that often co-occurs with seizures, anxiety, ataxia, motor skill deficits, and autism spectrum disorder (ASD) (3–5). The best characterized of these links is between the X-linked gene *KDM5C* and the intellectual disability disorder Claes–Jensen syndrome, for which at least 85 pathogenic genetic variants have been published (4,6,7).

The functions of KDM5 proteins are evolutionarily conserved, with studies in *Mus musculus*, *Drosophila melanogaster* and *Caenorhabditis elegans* revealing neuromorphological and behavioral characteristics consistent with reported human clinical phenotypes. For example, mice homozygous for knockout of *Kdm5a*, *Kdm5b* or hemizygous for loss of *Kdm5c*, show cognitive deficits, increased anxiety, seizure susceptibility and/or aggression (3,8–11). Similarly, the single *Kdm5* ortholog in *Drosophila* is important for locomotion during larval development and for cognitive function in adult flies (12,13). Changes to synaptic function and axonal growth and guidance are two potential contributors to KDM5-dependent changes to brain function (14,15). Indirect evidence of altered synaptic activity has been observed in *Kdm5c* knockout mice, where pyramidal neurons of the adult brain show reduced dendritic spine density, which could result in, or be caused by, altered synaptic activity (10,16). Direct evidence has come from *Drosophila*, where KDM5 is needed for proper morphology of synaptic boutons and neurotransmission at the glutamatergic larval neuromuscular junction (12). Studies using *Drosophila* and *C. elegans* have also revealed a role for KDM5 in axonal growth and guidance. In *C. elegans*, a loss of function allele of the single *Kdm5* ortholog leads to axonal guidance defects that correlate with altered F-actin polymerization dynamics (17,18). Similar findings have been observed in the *Drosophila* mushroom body, a learning and memory center of the adult fly, where reducing KDM5 levels during early neuronal differentiation results in mushroom body axonal mis-projection and overgrowth (19).

Although the neuromorphological consequences of KDM5 loss of function are beginning to be elucidated, the transcriptional and downstream cellular changes that underly altered synaptic and axonal structure and function are less clear. To date, there have been no transcriptional studies examining the consequences of loss of *KDM5* family genes in human neurons. Gene expression studies have, however, been carried out using the hippocampus and other regions of the brain from *Kdm5a* and *Kdm5c* knockout mice (8,9,11). These studies have revealed the dysregulation of genes known to be involved in neuronal function, but have not led to clear models of the pathways that link KDM5 protein function to ID. One candidate process has, however, emerged from genomic binding and gene expression studies carried out in *Drosophila*. Transcriptomic data using adult heads of flies harboring an allele comparable to an ID-associated variant in *KDM5C* showed decreased expression of genes related to cytoplasmic translation and ribosome biogenesis (13). Ribosome trafficking and proper localization of protein synthesis are key mechanisms necessary to regulate synaptic formation, maintenance, and function (20). Consistent with this, genetic variants in regulators of translation such as the Fragile X gene *FMR1* have been shown to alter the neuronal translatome, chiefly through the proximal translational silencing of distally trafficked mRNA (21,22). Thus, deficits in translation could contribute to KDM5-induced altered cognition. However, it remains to be determined whether altered expression of ribosomal protein genes is a common consequence of different ID-associated variants in *KDM5* genes, or whether this alters the neuronal translatome.

Here, we examine the link between KDM5-regulated transcription, regulation of translation, and altered neuronal development and function. Key to this study is five *Drosophila Kdm5* alleles that are analogous to *KDM5C* variants identified in individuals with Claes-Jensen syndrome. Analyses of these alleles revealed that loss of histone demethylase activity is not a universal feature of ID-associated variants, emphasizing the importance of non-enzymatic transcriptional activities of KDM5 proteins. ID-variants in *Kdm5* also disrupt neuronal development and function, leading to axonal growth and guidance defects, altered learning and/or memory, increased propensity for seizures, and altered locomotion. Molecularly, the brains of ID-allele fly strains show a signature pattern of altered gene expression that is characterized by reduced expression of genes encoding ribosomal proteins. A similar effect on ribosomal protein gene expression was observed in human induced pluripotent stem cell (iPSC)-derived glutamatergic neurons lacking *KDM5C*, indicating that this is an evolutionarily conserved function of KDM5 family proteins. In *Drosophila*, neuronal knockdown of *Kdm5* resulted in altered ribosome composition. Moreover, Ribo-Seq analyses revealed a decrease in the translation efficiency (TE) of transcripts encoding proteins necessary for mitochondrial metabolism, such as those involved in the tricarboxylic acid (TCA) cycle and fatty acid metabolism. This altered translation correlated with changes to neuronal metabolite concentrations, suggesting a new link between KDM5 and the maintenance of proper mitochondrial function in neurons. These studies uncover these new aspects of neuronal ribosome biology and provide a candidate pathway that could contribute to altered cognition and behavior across species.

Materials and methods

Fly strains and care

Fly food contained 80 g malt extract, 65 g cornmeal, 22 g molasses, 18 g yeast, 9 g agar, 2.3 g methyl para-benzoic acid and 6.35ml propionic acid per liter. Flies were kept at 25°C with a 12-h light/dark cycle and 50% humidity. The following fly stocks were obtained from Bloomington *Drosophila* Stock Center: w^{1118} (RRID:BDSC_5905), elav-Gal4 (RRID:BDSC_458), UAS-RpL3:FLAG (RRID:BDSC_77132), UAS-sh*Kdm5* (RRID:BDSC_35706). Alleles of *Kdm5* including $Kdm5^{\Delta}$ (null allele; previously known as $Kdm5^{140}$), $Kdm5^{JmjC*}$, $Kdm5^{A512P}$, $Kdm5^{L854F}$, $Kdm5^{R873W}$ and $Kdm5^{Y874C}$ are published

(12,13,23,24). The HA-tagged $Kdm5^{WT}$ fly strain has been shown to express KDM5 at endogenous levels (23). $Kdm5^{A224T}$ and $Kdm5^{D234G}$ were generated in the same manner as previous alleles using a clone of the 11 kb genomic region encompassing *Kdm5* locus from the end of the transcript of the upstream gene *Tsp26A* to the promoter of the downstream gene *ifc*, with an in-frame 3xHA tag at the 3′end (in the vector pattB; DGRC Stock 1420; https://dgrc.bio.indiana.edu//stock/1420;RRID:DGRC_1420). For $Kdm5^{A224T}$, codon 224 was changed from GCA to ACA by site-directed mutagenesis and codon 234 from GAT to ACT for $Kdm5^{D234G}$ (25). Sequenced constructs were sent to BestGene Inc for injection into FlyC31 embryos (RRID:BDSC_24749; attP86F). Transformed flies were crossed into the $Kdm5^{\Delta}$ null mutant background. For all assays except habituation, male and female flies used were homozygous for $kdm5^{\Delta}$ and homozygous for the genomic transgene such that the sole source of KDM5 was ID-variant (homozygous mutant). For habituation data, male flies heterozygous for $kdm5^{\Delta}$ and heterozygous for the genomic transgene were used.

Human cell line LS200 and generation of $KDM5C^{KO}$ lines

The LS200 iPSC line derived from a typically developing male has been previously described (26). The two *KDM5C* knockout lines were generated using Invitrogen TrueCut™ Cas9 Protein v2 (Invitrogen_A36496) and Invitrogen™ TrueGuide™ Synthetic gRNA (Invitrogen_A35509). Ribonucleoprotein transfection was performed by electroporation using the Invitrogen™ Neon Transfection System (Invitrogen_MPK1025) according to the protocol provided by the manufacturer. The transfection reaction consisted of 1.5 μg of Cas9 and 300 ng of sgRNA using pre-set program 7. After recovery, iPSCs were expanded and genome editing was assessed using the GeneArt™ Genomic Cleavage Detection Kit (Invitrogen_A24372). Once successful cleavage was determined, iPSCs were FACS-sorted using a BD FACSAria™ IIu Cell Sorter and allowed to grow at 1 cell per well in a 96-well plate. Knockouts were verified by PCR and Sanger sequencing.

Generation of iPSC-derived glutamatergic neurons

iPSCs were maintained as previously described (26,27). Glutamatergic neuronal differentiation was induced using a protocol developed by Zhang *et al.*, in which differentiation is driven by overexpression of the transcription factor Neurogenin2 (NGN2) (27). A tet-inducible expression system was introduced, and lentivirus particles prepared from the plasmid vectors; pLV_TRET_hNgn2_UBC_Puro (RRID:Addgene_61474) and FUdeltaGW-rtTA (RRID:Addgene_19780), followed by treatment with doxycycline and selection with puromycin.

Antibodies

The following primary antibodies were used: Anti-Fas2 (1:25, Developmental Studies Hybridoma Bank (DSHB) cat# 1D4 anti-Fasciclin II, RRID:AB_528235), Anti-HA (1:1000, Cell Signaling Technology cat# 3724, RRID:AB_1549585), anti-H3 (1:20000, Active Motif Cat# 39763, RRID:AB_2650522), anti-H3K4me3 (Cell Signaling Technology Cat# 9751, RRID:AB_2616028), Anti-FLAG (Sigma-Aldrich Cat# F1804, RRID:AB_262044), Anti-vGLUT2 (1:200; Millipore #mab5504) Anti-TUJ (1:500; Genescript #A01627), Anti-Cyclophilin B (Thermofisher #PA1-027A), anti-DAC (1:50; DSHB cat# mAbdac2-2; RRID:AB_528190). Anti-RpS12 was a gift from Dr. Nicholas Baker (Albert Einstein College of Medicine) (28). Anti-KDM5C was a gift from Dr Shigeki Iwase (University of Michigan) (8). Secondary antibodies: Goat anti-mouse Alexa-488 (1:500, Thermo Fisher Scientific cat# A32723; RRID:AB_2633275), IRDye 680RD donkey anti-mouse IgG (1:8000; LI-COR Biosciences cat# 925-68072, RRID:AB_2814912) and IRDye 800CW donkey anti-rabbit IgG (1:8000; LI-COR Biosciences cat# 926-32213, RRID:AB_621848). Blots were scanned and processed using a LI-COR Odyssey Infrared scanner and band intensities quantified with ImageJ (29).

Immunohistochemistry

Drosophila

For adult brains whole flies were fixed in 4% paraformaldehyde in phosphate buffered saline (PBS) with 0.2% Triton X-100 (0.2% PBT) at 4°C for 3 h and then washed in 0.2% PBT for three cycles of 15 min at room temperature (RT). Brains were next dissected in 0.2% PBT, blocked for 30 min at RT (5% normal goat serum in 0.2% PBT) and incubated with primary antibodies prepared in 5% NDS/0.2% PBT for 2 days at 4°C. After three cycles of 15 min in 0.2% PBT washing, secondary antibodies were added for 1–2 days at 4°C. After being washed in PBS for three cycles of 15 min at RT, brains were incubated in a drop of Vectashield mounting medium (Vector Laboratories, H-1000) or DAPI Fluoromount G (SouthernBiotech, OB010020) overnight at 4°C. Brains were mounted on glass slides (Superfrost Plus, Fisherbrand), flanked by glass spacers, and covered with a final glass coverslip prior to image analysis. Images were taken on a Leica SP8 confocal microscope using either a ×20 air lens (N.A. = 0.75 air, W.D. = 0.64 mm) or a ×63 immersion lens (N.A. = 1.4 oil, W.D. = 0.14 mm). Confocal stacks were taken under either ×2 or × 2.5 zoom, in a 1024 × 1024 configuration and using 1μm resolution. Image stacks were processed with Fiji (ImageJ). For statistical tests of mushroom body morphological defects, a chi-squared test followed by Mariscuillo procedure was performed using GraphPad Prism 8.4 (GraphPad Software, Inc., CA, USA) and R.

Human iPSC-induced glutamatergic neurons

Staining of iNeurons was carried out as described in Barnes *et al.* (26). iNeurons were grown to day 21 on 12 mm coverslips coated with Laminin. Cells were fixed in 10% buffered formalin phosphate for 10 min at 4°C, and permeabilized at RT for 15 min with 1% Triton X-100 in PBS. Samples were blocked using 5% donkey serum/1% bovine serum albumin (BSA)/1% Triton-X100 for 45 min at RT and primary antibody added and incubated for 1 h at RT. Samples were washed several times in 5% donkey serum/1% BSA prior to secondary antibody incubation for 45 min at RT. Samples were washed several times prior to addition of ProLong Gold antifade reagent with DAPI (Invitrogen #P36931). Images were taken on a Leica SP8 confocal microscope using a ×40 immersion lens.

Appetitive olfactory learning and memory assay

Single-round training appetitive learning and memory assays were carried out similarly to protocols described previously, using 3- to 5-day-old flies and a T-maze purchased from Cel-

Explorer Labs (30). All tests were performed in the afternoon (1–3 p.m.) at a temperature of room temperature and >40% humidity. Flies were starved in vials along with a filter paper disk soaked in water for 16–20 h prior to training. Single-round training was performed by placing flies in a chamber along with a filter paper square that had been soaked with water and allowed to air dry. Odor from a solution of 3-octanol (3-OCT) diluted in mineral oil at 1:1000 was infused into the chamber simultaneously at a flow rate of 1 l/min for 2 min. Room air was then infused into the chamber for 30 s. Flies were subsequently transferred to another chamber along with a filter paper that was previously soaked with 2 M sucrose and allowed to air dry. Odor from a solution of 4-methylcyclohexanol (4-MCH) diluted in mineral oil at 1:1000 was infused into the chamber simultaneously at a flow rate of 1 l/min for 2 min. Flies were then placed on standard food for 30 min before being starved for 24 h with a filter paper disk soaked in water. For testing, flies were placed in a T-maze. Odors from the same 3-OCT and 4-MCH solutions were infused from each arm of the T-maze at a flow rate of 1 l/min for 2 min in complete darkness and flies were allowed to enter and traverse each arm of the T-maze. After 2 min, flies were removed from each arm of the T-maze and quantified. Memory was quantified using a performance index (PI) calculated by subtracting the number of flies avoiding sucrose-associated odor from the number of flies preferring the sucrose-associated odor and dividing by the total number of flies. Each experiment was carried out a minimum of six times per genotype.

Habituation assay

Habituation learning was tested with the high-throughput light-off jump habituation assay (31). To generate white-eyed genomic rescue transgenes for ID-*Kdm5* variants, as required for the efficient jump response to the light-off stimulus, we excised the *white* gene cassette using the CRE recombinase. Three-to-four-day old males were individually placed in semi-transparent vials enclosed by two microphones of two independent 16-unit light-off jump habituation systems (Aktogen Ltd.) and left to acclimatize for 5 min before starting the habituation paradigm assay in which 32 flies were simultaneously exposed to 100 light-off pulses of 15 ms with a one second inter-trial-interval. The noise amplitude produced by wing vibrations was recorded for 500 ms after each light-off pulse. The obtained sound amplitudes were filtered with a threshold to remove background noise, leading to the annotation of a jump at amplitude above 0.8 V. Jump quantitation were collected and analyzed by a custom-made Labview Software (National instruments). A high initial jump response to the light-off pulse decreased with the repetition of pulses. Flies were considered habituated when they failed to jump to five consecutive trials (no jump criterion). The number of trials required to reach the no jump criterion (trials to habituation, TTC) was collected for each individual fly. The effect of genotype on log transformed TTC values, corrected for the effect experimental day and system, was analyzed with a linear model in the R statistical software (v.3.0.0). Resulting *P*-values were corrected for multiple comparisons with Bonferroni–Holm method (P_{adj}).

Mechanically induced seizure assays

The protocol for mechanical seizure induction was adapted from Mituzaite et al (32). Flies <7 days old were separated under carbon dioxide anesthetization into groups of seven or fewer in individual food-containing vials. Animals were allowed to recover overnight before being transferred without anesthetization to empty testing vials. After transfer, flies were left to acclimatize for at least an hour before testing. During the vortex assay, flies were shaken at maximum speed in their vials on a laboratory vortex for ten seconds. Vials were then moved to a tube holder and recorded for five minutes using a smartphone camera. All testing was done during the morning hours. Recordings were used to visually track each fly for 5 min to note all seizures. Bang-sensitive *Drosophila* go through a stereotypic seizure cycle during which the fly may turn onto its side or back and exhibit behaviors such as shaking and paralysis. (33) Similar numbers of males and females were used for each variant tested. Statistical analysis was done using a Chi-Square Test in GraphPad PRISM 8.4 (GraphPad Software, Inc., CA, USA) followed by a Marascuilo procedure to adjust for multiple comparisons, which was done in R.

Locomotion

The protocol for quantifying locomotion assay was adapted from Mi *et al.* (34). Seven to ten male or female flies less than seven days old were anesthetized and portioned into vials containing standard fly medium 24 h prior to testing. On the day of testing, flies were individually aspirated into the testing chambers, and were left to acclimate for an hour before video recording for 5 min. Flies were tracked post hoc in videos using UMA tracker and analyses of tracking was completed in R Studio (35). Dunnett's one way ANOVA was used to account for multiple comparisons.

RNA-Seq

Drosophila

The $Kdm5^{JmjC*}$ RNA-seq dataset is published (GEO:GSE100578) (13). For the remaining genotypes, RNA was prepared from 3–5 day old heads during the morning hours using Trizol. $Kdm5^{JmjC*}$, $Kdm5^{L854F}$ and $Kdm5^{A224T}$ libraries were prepared using the TruSeq Stranded mRNA Library Preparation Kit. Samples were sequenced on an Illumina HiSeq2500 sequencer (v4 chemistry) using 2 × 50 bp cycles. Genotypes $Kdm5^{D234G}$, $Kdm5^{R873W}$ and $Kdm5^{Y874C}$ were sequenced with Novogene with Illumina HiSeq sequencer in triplicate, accompanied by two $Kdm5^{WT}$ samples for used for batch correction. Raw reads of all genotypes were aligned with RSubread (v2.10.5), normalized, and differential expression determined with DESeq2 (v1.38.3) (36).

Human cells

Total RNA from day 45 glutamatergic neurons was extracted from each of the duplicate samples of matched control and $KDM5C^{KO}$ cell lines using the Qiagen miRNeasy Mini kit (#217002). Libraries were prepared by Novogene for 150 bp paired-end (PE) sequencing in an Illlumina HiSeq platform. PE reads were aligned to the human reference sequence hg38 using STAR (v2.7.9a). (37) RSEM (v1.3.3) was used to compute read count, fragments per million fragments mapped (FPKM) and transcripts per million (TPM) for all genes annotated in the GENCODE database (v41). (38,39) Genes with a TPM of ≥1 in at least one sample was used for subsequent studies. DEseq2 (v1.38.3) was used for differential gene expression analyses by combining duplicate samples from each knockout such that the final analyses compared four control to four $KDM5C^{KO}$ samples (36).

Ribo-seq

For Ribo-Seq we followed the protocols outlined in Chen *et al.* (40). This experiment was performed in biological triplicate. 200 flies per sample were flash frozen, decapitated, and homogenized in lysis solution (10 mM HEPES, pH 7.4, 150 mM KCl, 5 mM $MgCl_2$, 100 μg/ml cycloheximide) supplemented with 0.5% Triton-X100, 1 U/ul SUPERase•In™ RNase Inhibitor (ThermoFisher, AM2694) and Halt™ Protease Inhibitor Cocktail (Thermofisher, 78430). Anti-Flag antibodies (Sigma, F1804) were bound to Dynabeads Protein G (ThermoFisher, 10004D) as per manufacturer's specifications. Lysate was centrifuged at 4°C for 10 min at 15 000×g. The supernatant was added to the beads and supplemented with 200 000 U of RNAse T1 (Thermofisher, EN0541) and incubated with rotation at 4°C for 6 h. Afterwards the supernatant was discarded, and the beads were washed three times with wash buffer (10 mM HEPES, pH 7.4, 150 mM KCl, 5 mM $MgCl_2$, 100 μg/ml cycloheximide). RNA was eluted from the beads using Trizol (Invitrogen, 15596026). Immunoprecipitated RNA was sent to Novogene for library preparation and sequencing. The ORFik package was used for mapping and Ribo-Seq analysis (41). We detected few changes to RFP, mRNA, or TE levels between alternate transcripts derived from the same gene, so we elected to use genes for downstream analyses.

Immunoprecipitation followed by mass spectrometry

We immuno-precipitated ribosomes using the same protocol as above without RNase T1 in triplicate. After washing the ribosomes, samples were sent for mass spectrometry analyses.

On-bead protein digestion

Proteins were digested directly on streptavidin beads. 5 mM DTT and 50 mM ammonium bicarbonate (pH 8) were added to the solution and left on the bench for about 1 hour for disulfide bond reduction. Samples were then alkylated with 20 mM iodoacetamide in the dark for 30 min. Afterward, 500 ng of trypsin was added to the samples, which were digested at 37°C for 18 h. The peptide solution was dried in a vacuum centrifuge.

Sample desalting

Prior to mass spectrometry analysis, samples were desalted using a 96-well plate filter (Orochem) packed with 1 mg of Oasis HLB C-18 resin (Waters). Briefly, the samples were resuspended in 100 μl of 0.1% trifluoroacetic acid and loaded onto the HLB resin, which was previously equilibrated using 100 μl of the same buffer. After washing with 100 μl of 0.1% TFA, the samples were eluted with a buffer containing 70 μl of 60% acetonitrile and 0.1% TFA and then dried in a vacuum centrifuge.

LC–MS/MS acquisition and analysis

Samples were resuspended in 10 μl of 0.1% TFA and loaded onto a Dionex RSLC Ultimate 300 (Thermo Scientific), coupled online with an Orbitrap Fusion Lumos (Thermo Scientific). Chromatographic separation was performed with a two-column system, consisting of a C-18 trap cartridge (300 μm ID, 5 mm length) and a picofrit analytical column (75 μm ID, 25 cm length) packed in-house with reversed-phase ReproSil Pur C18-AQ 3 μm resin. Peptides were separated using a 90 min gradient from 4% to 30% buffer B (buffer A: 0.1% formic acid, buffer B: 80% acetonitrile + 0.1% formic acid) at a flow rate of 300 nl/min. The mass spectrometer was set to acquire spectra in a data-dependent acquisition (DDA) mode. Briefly, the full MS scan was set to 300–1200 m/z in the orbitrap with a resolution of 120 000 (at 200 m/z) and an AGC target of 5 × 10e5. MS/MS was performed in the ion trap using the top speed mode (2 s), an AGC target of 1 × 10e4 and an HCD collision energy of 35.

Raw files were searched using Proteome Discoverer software (v2.4, Thermo Scientific) using SEQUEST search engine and the UniProt database of *Drosophila melanogaster*. The search for total proteome included variable modification of N-terminal acetylation, and fixed modification of carbamidomethyl cysteine. Trypsin was specified as the digestive enzyme with up to 2 missed cleavages allowed. Mass tolerance was set to 10 pm for precursor ions and 0.2 Da for product ions. Peptide and protein false discovery rate was set to 1%. Following the search, data was processed as described by Aguilan *et al.* (42). Briefly, proteins were $\log_2$ transformed, normalized by the average value of each sample and missing values were imputed using a normal distribution 2 standard deviations lower than the mean. Statistical regulation was assessed using heteroscedastic t-test (if P-value < 0.05). Data were assumed to be normally distributed.

Metabolomics

Fifty heads per sample were flash frozen in liquid nitrogen in quadruplicate. The samples were added 200 ul of 80% methanol with internal standards in a bead's beater. The samples were centrifuged at 14 000 rpm for 10 min, the supernatant was transferred into glass vials for injection. The samples were analyzed with ABsciex 6500+ with Ace PFP column. A pooled quality control (QC) sample was added to the sample list. This QC sample was injected six times for coefficient of variation (CV) calculation for data quality control. CVs lower than 20% were treated as accurate quantification, CVs between 20% and 30% were treated as relatively accurate quantification, while CVs higher than 30% were treated as inaccurate data. 334 metabolites were detected with a CV <30% in the QC samples. The dataset imported into SIMCA-p software (Umeå, Sweden) for multivariate analysis. For analyses, fold changes of mass abundances normalized to a single control.

MetaboAnalyst

The online tool MetaboAnalyst 6.0 was used to perform joint pathway analyses on differential metabolites and translationally regulated mRNAs (43). Options were as follows: all pathways (integrated), enrichment analysis: hypergeometric test, topology measure: degree centrality, and integration method: combine queries.

Results

Generation of *Drosophila Kdm5* alleles equivalent to intellectual disability-associated variants in *KDM5C*

Claes-Jensen syndrome-associated missense variants in *KDM5C* occur in amino acids that are conserved in *Drosophila* KDM5. Compared to analyses of complete

loss of KDM5, single amino acid changes may alter a subset of its functions to reveal target genes and pathways that are relevant to the pathomechanisms of Claes–Jensen syndrome. We therefore utilized five patient intellectual disability (ID)-associated missense variants at the analogous residue in *Drosophila* KDM5, three of which we previously used to examine larval neuromuscular junction phenotypes (12). These variants occur within several different KDM5 domains and are associated with a range of ID severity and co-occurring features such as epilepsy, ataxia, aggression, and short stature (Figure 1A) (7,44–46). One of these alleles, $Kdm5^{D234G}$, is the only variant identified in two unrelated families, and another is notable in that the equivalent amino acid is altered in *KDM5C*- and *KDM5A*-associated ID ($Kdm5^{R873W}$) (7,46). Our analyses also include a synthetic demethylase dead allele ($Kdm5^{JmjC^*}$) to assess the role of the enzymatic function of KDM5 (12,23,24,47). We have previously shown that the ID-allele $KDM5C^{A388P}$, $Kdm5^{A512P}$ in *Drosophila*, behaves indistinguishably from $Kdm5^{JmjC^*}$ with respect to gene expression changes in addition to neuronal and behavioral phenotypes (13).

ID allele strains were created by combining a *Kdm5* null allele ($Kdm5^{\Delta}$) with a transgene encoding a HA-tagged form of the entire wild-type ($Kdm5^{WT}$) or $Kdm5^{ID\text{-}variant}$ locus at chromosomal location 86F (Supplementary Figure S1A). In contrast to loss of *Kdm5*, $Kdm5^{\Delta}$ animals re-expressing ID-variant proteins were homozygous viable, suggesting that these alleles disrupt a subset of KDM5's gene regulatory activities. To confirm that ID-variant proteins were expressed at wild-type levels, we carried out western blots to detect HA-tagged KDM5 using total protein from adult heads (Figure 1B). We also indirectly examined the effect of ID-variants on histone demethylase activity by quantifying bulk levels of H3K4me3 relative to total histone H3 (Figure 1C, D). This revealed that $Kdm5^{D234G}$, $Kdm5^{L854F}$, $Kdm5^{R873W}$ and $Kdm5^{Y874C}$ did not affect levels of H3K4me3, suggesting that they retain demethylase activity. $Kdm5^{A224T}$ was the only ID-variant strain that showed a two-fold increase to H3K4me3 levels similar to that observed for $Kdm5^{JmjC^*}$, indicating a loss of demethylase function (Figure 1C-D). We also verified that all ID-variant forms of KDM5 were properly localized to the nucleus by immunostaining adult brains (Supplementary Figure S1B).

ID-variant fly strains display neuromorphological and behavioral phenotypes

In previous work, we found that 70% of $Kdm5^{\Delta}$ pharate adult animals exhibit axonal growth and guidance defects of the α and β lobes of the mushroom body, an integrative signaling center of the *Drosophila* brain (19). This was not seen in $Kdm5^{JmjC^*}$ animals, showing that KDM5 is needed for proper axonal development independently of its histone demethylase activity (13). To determine the extent to which other ID-variants altered mushroom body structure, we performed immunohistochemical staining of the α and β lobes using Fas2 as a marker (Figure 1E). This revealed that all alleles showed neuromorphological defects, ranging from 8% of brains in $Kdm5^{D234G}$ animals to 33% in $Kdm5^{R873W}$ (Figure 1F). Interestingly, defects were seen in $Kdm5^{A224T}$ flies that lack enzymatic activity, clearly distinguishing this allele from the demethylase dead $Kdm5^{JmjC^*}$ strain which does not alter mushroom body morphology (13). The $KDM5^{A224T}$ protein is therefore likely to be deficient in more than one KDM5 function.

We have previously shown that $Kdm5^{JmjC^*}$ animals show defects in short- and long-term memory (13). To understand the extent to which each ID-variant affects memory formation and/or recall, we performed appetitive olfactory learning and memory assays. In these assays, water or a sugar reward are paired with octanol (OCT) or 4-methylcyclohexanol (MCH), and the ratio of flies recalling the sugar-paired odor is calculated as the performance index (PI). In the absence of training, all strains showed a similar slight preference for MCH over OCT (Figure 1G). After a single round of training, $Kdm5^{D234G}$ and $Kdm5^{L854F}$ animals showed significant or trending deficits in both short- and long-term memory (Figure 1H-I). $Kdm5^{A224T}$ animals showed variable short-term memory performance, for which the mean PI was not significantly different than controls, but profound long-term memory deficits. Conversely, $Kdm5^{Y874C}$ showed mild short-term learning changes ($P = 0.07$) but no detectable change to long-term memory.

Drosophila models of ID are frequently characterized by deficits in habituation, which allows organisms to adapt to and ultimately ignore familiar, irrelevant stimuli, preserving cognitive capacities (31,48,49). In the light-off jump habituation paradigm, many ID models fail to suppress their jump response to repeated light-off stimuli, paralleling habituation deficits to different modalities reported in individuals with ASD and monogenic ID syndromes (31,50). Homozygous ID-variant expressing flies did not show a robust response to light-off stimuli, thus we used animals heterozygous for both $Kdm5^{\Delta}$ and the ID-variant transgenic rescue construct for these studies. Using this strategy, flies expressing the $Kdm5^{WT}$ rescue construct showed a steep adaptation to the repeated stimulus, as expected. Quantifying the number of trials that are required to reach the no-jump criterion (Trials to Criterion; TTC), this genotype habituated with a low mean TTC. In contrast, the mean TTCs of all ID-variant strains tested was significantly greater, demonstrating an incomplete rescue of habituation for these variants compared to the $Kdm5^{WT}$ (Supplementary Figure S2A-E). Combined with the learning and memory assays, these data show that ID-variants disturb *Kdm5* function and lead to cognitive dysfunction.

In addition to cognitive changes, other frequently reported features of Claes–Jensen syndrome are epilepsy and ataxia/altered motor control (4,5,7). Seizures are reported in 80% of Claes-Jensen syndrome patients with *KDM5C* alleles predicted to be complete loss of function, and in about half of individuals with missense variants (4). Of the ID-allele fly strains generated, $Kdm5^{A224T}$ and $Kdm5^{D234G}$ are analogous to variants identified in individuals with documented seizure disorders (44,46). To test the extent to which ID-variant fly strains show seizure predisposition, we used a well-established paradigm that subjects flies to mechanical stress (32). In this assay, flies are vortexed at maximum speed and the number that show seizure-like behavior within five minutes counted. Comparing the ID-variant and control groups revealed a consistent 2-fold or greater increase in seizure susceptibility across all variant fly stains (Figure 1J). To assay movement in flies, we quantified distance traveled and median speed of adult flies over a 5-minute period and found that all ID-variant and $Kdm5^{JmjC^*}$ animals exhibited a reduction in both (Figure 1K, L). Representative tracings are shown in Supplementary Figure S2F. Combined, these data are con-

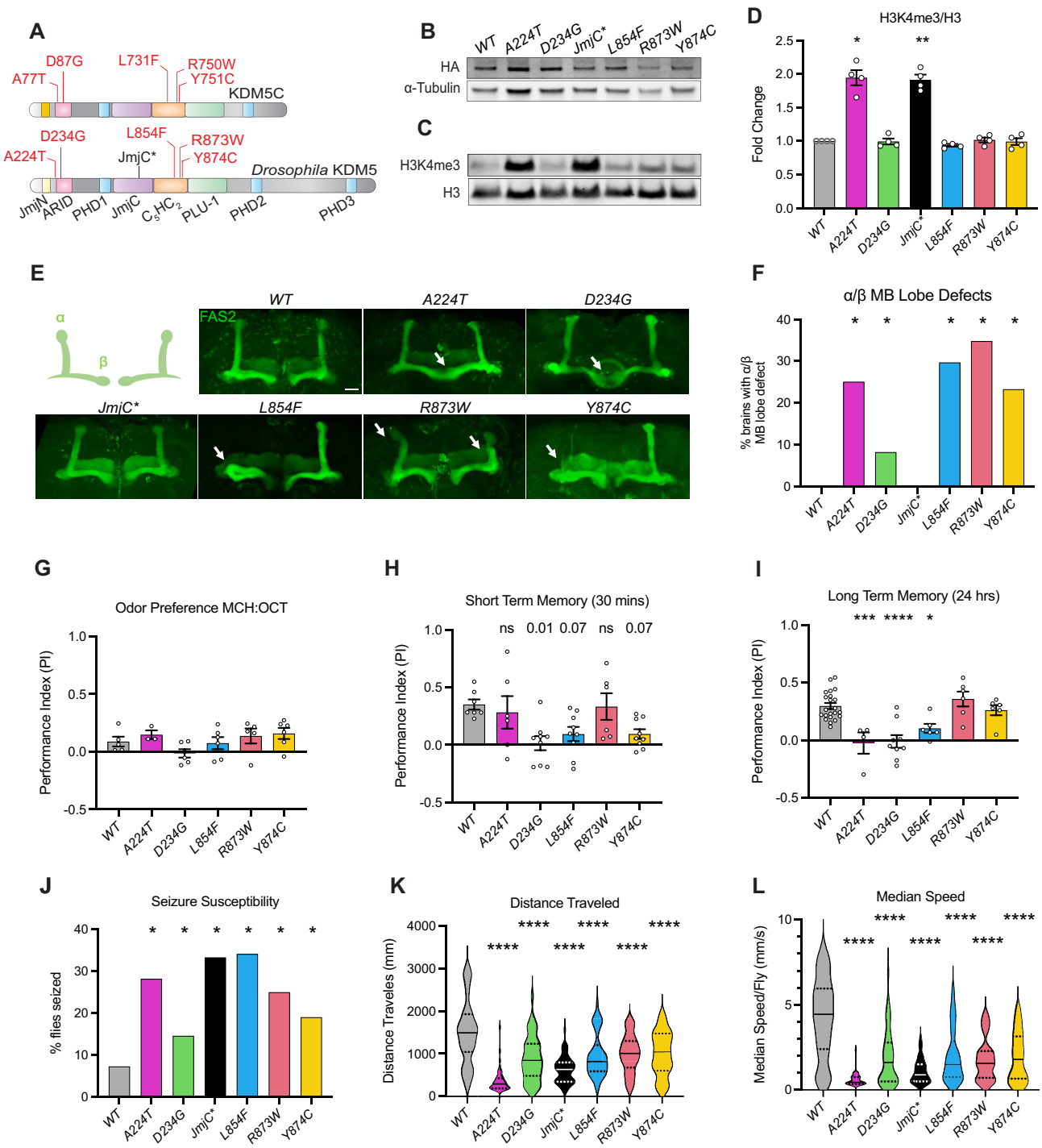

Figure 1. ID-associated variants in *Drosophila Kdm5* show altered neuronal development and function. (**A**) A schematic of human KDM5C patient ID-associated missense variants and their analogous conserved residues in *Drosophila melanogaster* KDM5. (**B**) Western blot of HA-tagged KDM5 shows that ID-variants do not affect protein levels. α-tubulin used as loading control. All flies are homozygous for $Kdm5^{\Delta}$ and for the ID-variant encoding transgene such that the sole source of KDM5 is from the transgene. Genotypes indicated above blot. (**C**) Western blot of adult heads from control and ID-variant strains probed with antibodies toward H3K4me3 and total H3 as loading control. Genotypes identical to panel B. (**D**) Quantification of H3K4me3:H3 ratios, $N = 4$. $Kdm5^{A224T}$ and $Kdm5^{JmjC*}$ show increased bulk H3K4me3 relative to total H3 while the other alleles do not. (**E**) Anti-Fas2 immunofluorescent staining to visualize the alpha (α) and beta (β) lobes of the mushroom body to reveal morphogenesis defects in ID-variant adult brains. Arrows indicate morphological defects. $N = 35$ for all genotypes. Scale bar represents 20 μm. (**F**) Quantification of the number of animals showing mushroom body defects. Chi squared test followed by Marascuilo procedure. (**G**) Preference for 4-methylcyclohexanol (MCH) compared to octanol (OCT) in the absence of training. (**H**) Short term memory assay carried out 30 min after training. (**I**) Long term memory assay carried out 24 h after training. (**J**) Percentage of flies for each genotype that had one or more seizures following mechanical stress. $N = 41$ (WT), 39 (A224T), 41 (D234G), 42 (JmjC*), 41 (L854F), 40 (R873W), 42 (Y874C). (**K**) Total distance traveled in millimeters (mm) for each genotype in 5 min. Numbers of flies used were WT $N = 48$, A224T $N = 42$, D234G $N = 40$, JmjC* $N = 49$, L854F $N = 49$, R873W $N = 41$, Y874C $N = 43$. (**L**) Median speed (mm/second) for each genotype using same animals as in (K). Statistics: one-way ANOVA or Chi-squared test followed by Marascuilo procedure performed when appropriate. *P*-values *<0.05, **<0.01, ***<0.001, ****<0.0001.

sistent with KDM5 playing roles in suppressing seizures and in facilitating typical locomotion.

KDM5 is needed to maintain the expression of ribosomal protein genes in *Drosophila* and in human iNeurons

To define the common and divergent pathways altered by each ID-variant, we performed RNA-sequencing (RNA-seq) analyses using adult heads and integrated these with our previously generated $Kdm5^{JmjC*}$ data (Supplementary Table S1) (13). Principal component analysis (PCA) of batch-corrected data show two distinct clusters, $Kdm5^{A224T}$, $Kdm5^{JmjC*}$, and $Kdm5^{L854F}$ and $Kdm5^{D234G}$, $Kdm5^{R873W}$ and $Kdm5^{Y874C}$ (Figure 2A). Interestingly, 78% of the variance was found in PC1, suggesting converse gene expression changes among the two clusters. It is also notable that the $Kdm5^{L854F}$ allele that retains demethylase activity clusters with demethylase dead $Kdm5^{JmjC*}$ and $Kdm5^{A224T}$ alleles, suggesting that the loss of different KDM5 activities can lead to similar gene expression outcomes. Across all genotypes, several thousand differentially expressed genes (DEGs) were observed using a 5% FDR cutoff that were evenly distributed between upregulated and downregulated (Supplementary Figure S3A–F). These data are consistent with KDM5 having activating and repressing roles in gene expression, as has been observed previously (12,19,51). Also in keeping with prior studies of KDM5, ID-variants showed modest changes to gene expression, with mean log2FCs of 1.6 and –1.13 for upregulated and downregulated genes, respectively (Supplementary Figure S3; Supplementary Table S1).

To detect common gene expression signatures, we performed gene ontology (GO) analyses on DEGs. Across all datasets, terms relating to translation and ribosomes were the most significantly enriched, although this was less pronounced for $Kdm5^{R873W}$ and $Kdm5^{Y87C}$ (Figure 2B, C; Supplementary Figure S3G, H). A similar enrichment was seen in our previous gene expression study of $Kdm5^{\Delta}$ larval neuronal precursors and immature neurons, but not from our prior study of epithelial wing imaginal discs, suggesting that this gene expression signature may occur primarily in neurons (Figure 2G) (19,23). Key among the commonly altered genes in ID-variant and $Kdm5^{JmjC*}$ flies were ribosomal protein genes (RPGs) whose protein products are necessary for the proper formation and function of the ribosome. RPGs were downregulated across all genotypes, implicating wild-type KDM5 in the activation of these genes (Supplementary Figure S4A–H). RPGs are one of the most abundant classes of transcript, thus the modest ≤2-fold change to gene expression seen reflects a relatively large change to number of mRNAs present (red dots in Supplementary Figure S4I–P).

KDM5 is likely to directly regulate genes related to ribosomal function, as GO analyses of published genomic binding data from whole adults and neuronal precursors/immature neurons reveal an enrichment for this class of gene (Figure 2D, E) (19,51). Of the 93 RpS and RpL genes represented across our datasets, 73 were bound by KDM5 in ChIP-seq data from whole adults, 56 were bound in targeted DamID from neuronal precursors/immature neurons, and 48 were bound in both datasets (Figure 2F-G). These data also emphasize the fact that alleles that do (e.g. $Kdm5^{JmjC*}$) and do not (e.g. $Kdm5^{L854F}$) abrogate the histone demethylase activity of KDM5 lead to similar lowering of RPG expression. This suggests that both enzymatic and non-enzymatic activities of KDM5 are likely to be important for the regulation of these genes.

To test if KDM5-mediated regulation of RPGs is conserved in human cells, we used iPSC-induced excitatory glutamatergic neurons (iNeurons). Using a well-characterized iPSC line developed from a typically developing male, we generated two independent *KDM5C* knock out ($KDM5C^{KO}$) lines by targeting exon 3 using CRISPR-Cas9 (26). The $KDM5C^{13}$ allele has a 16bp insertion and the $KDM5C^{22}$ allele has a 4bp deletion, both of which lead to the introduction of a premature stop codon (Figure 3A). For each allele, we used a matched control parental strain that was subjected to the CRISPR-Cas9 mutagenesis protocol but had no change to the *KDM5C* gene. Consistent with expectations based on the molecular lesions, western blot analyses of $KDM5C^{KO}$ iPSC lines demonstrated the absence of KDM5C protein (Figure 3B). To confirm the ability of induced $KDM5C^{KO}$ glutamatergic neurons to differentiate, we showed that they have similar morphology and expression of the vesicular glutamate transporter 2 (VGLUT2) marker and neuronal β-tubulin III (TUJ1) to control cells (Figure 3C). For RNA-seq analyses, we used day-45 iNeurons to compare each $KDM5C^{KO}$ line to its control in duplicate. As expected, PCA analyses showed clear clustering of all $KDM5C^{KO}$ and all control samples, allowing us to combine the data to carry out differential gene expression using quadruplicate samples (Figure 3D). This revealed the upregulation of 495 genes while 348 genes were downregulated using a 5% FDR cutoff. (Figure 3E, F; Supplementary Table S2). GO analyses revealed that terms associated with translation and ribosome biogenesis were enriched among the downregulated genes, with 27 of the 86 detected RPGs being significantly affected (Figure 3G, H). The ability of KDM5 family proteins to promote RPG expression in neurons is therefore evolutionarily conserved.

Neuron-specific knockdown of *Kdm5* results in altered ribosome composition and globally reduced translation efficiency

To understand how KDM5-dependent changes to RPG expression affect downstream ribosome composition and translation efficiency (TE) in the *Drosophila* adult brain, we utilized a UAS-transgene encoding FLAG-tagged RPL3 (40,52). The RPL3:FLAG expressed from this transgene properly integrates into ribosomes and can be used to immunoprecipitate intact ribosome-mRNA complexes (52). To confine our analyses to KDM5 function within neurons, we took a RNA interference (RNAi) knockdown approach using a UAS-short hairpin transgene that efficiently reduces levels of KDM5 protein (UAS-$Kdm5^{RNAi}$) (19,53). To examine RPL3:FLAG containing ribosomes in neurons with decreased KDM5 we simultaneously expressed the RPL3:FLAG and $Kdm5^{RNAi}$ transgenes using the pan-neuronal driver elav-GAL4 (Figure 4A). Western blot analyses of adult heads showed that elav-GAL4 drives robust expression of RPL3:FLAG, and that KDM5 is reduced only in the strain expressing the $Kdm5^{RNAi}$ transgene (Figure 4B).

To confirm that pan-neuronal *Kdm5* knockdown in the context of RPL3:FLAG overexpression led to reduced levels of RPG mRNAs, we performed RNA-seq using adult heads. Compared to control animals expressing RPL3:FLAG alone, those co-expressing $Kdm5^{RNAi}$ in neurons using elav-GAL4 showed an upregulation of 1149 genes and downregulation of

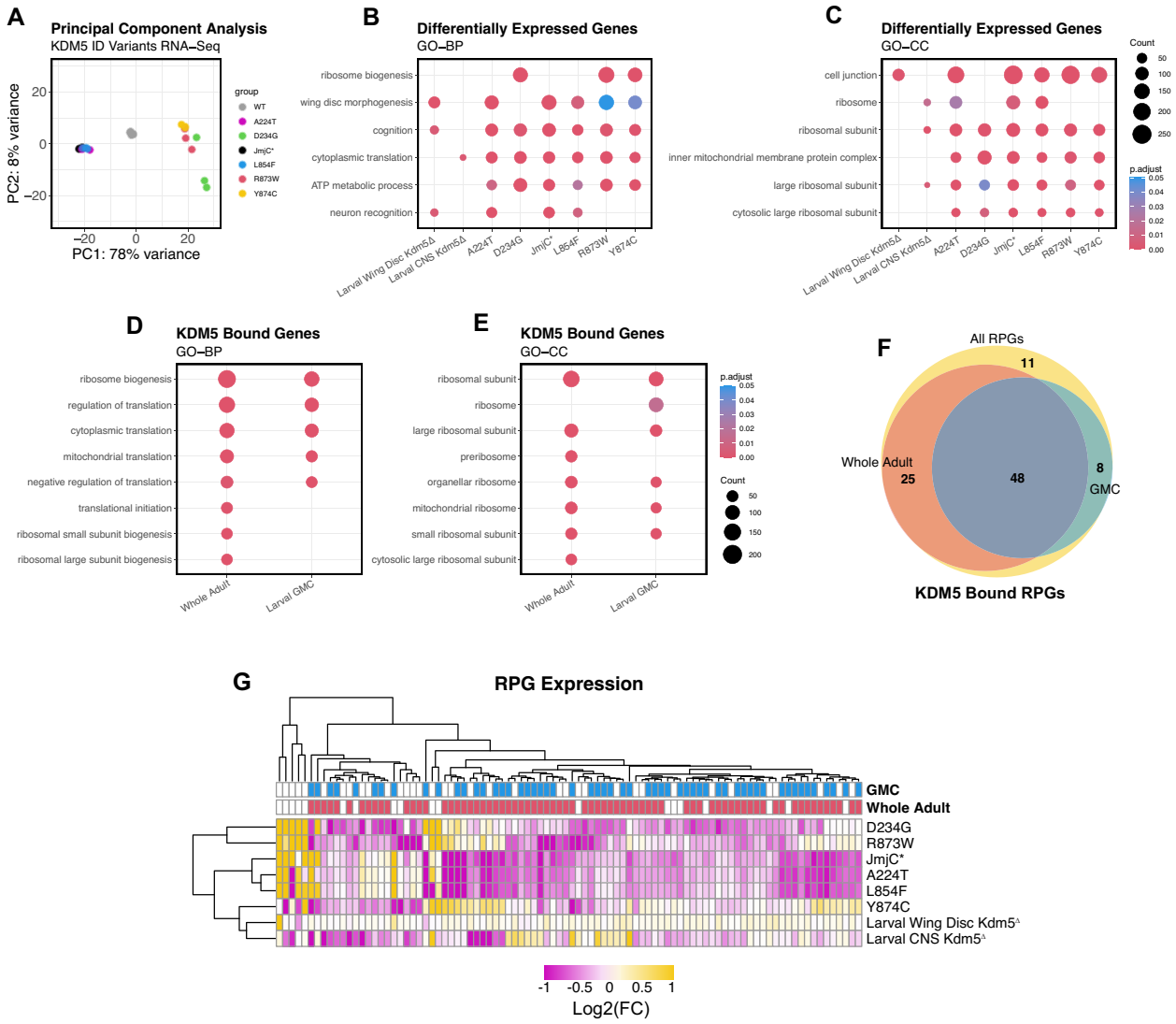

Figure 2. KDM5 is necessary for neuronal ribosomal protein gene expression. (**A**) Principal component analysis (PCA) plot of RNA-seq from heads of homozygous ID-variants performed in triplicate shows divergent expression patterns between *Kdm5*^{A224T}, *Kdm5*^{JmjC*} and *Kdm5*^{L854F} and *Kdm5*^{D234G}, *Kdm5*^{R873W} and *Kdm5*^{Y874C} datasets. (**B**) Gene ontology biological process (GO-BP) analyses of *Kdm5* mutant RNA-seq datasets show the term cytoplasmic translation is enriched in neuronal tissues. (**C**) Gene ontology cellular compartment (GO-CC) analyses of RNA-seq data show an enrichment of terms relating to ribosomal proteins in neuronal tissues. (**D**) GO-BP of KDM5 bound genes across tissue types shows recruitment to promoters of genes related to ribosomal function. (**E**) GO-CC of KDM5 bound genes also shows enrichment for ribosome related genes. (**F**) 81 out of 93 ribosomal protein genes (RPGs) are bound by KDM5 in ChIP-seq data from whole adults or TaDa from neuronal precursors (ganglion mother cells; GMC). (**G**) Heatmap of $\log_2$ (FC)s of RPGs across datasets shows downregulation of RPGs in neuronal tissues, but not in the wing imaginal disc. Yellow: up, purple: down. Blue: KDM5-Bound in GMC, Red: KDM5-Bound in whole adult.

1233 genes (5% FDR; Figure 4C; Supplementary Table S3). As expected, GO analyses of biological processes (GO-BP) and cellular compartments (GO-CC) of downregulated genes recapitulated data seen in ID-variants, where terms such as ribosome biogenesis and pre-ribosome were significantly enriched (Figure 4D, E). Looking specifically at RPG expression, 79 of 88 expressed RPGs were downregulated in response to reduced levels of KDM5 (Figure 4F). Thus, neuron-specific knockdown of *Kdm5* in adult heads results in a reduction in RPG expression that is not affected by RPL3:FLAG co-expression. Comparing affected RPGs across species revealed that 23 of the 29 RPGs downregulated in human *KDM5C*^{KO} glutamatergic neurons were also affected in *Drosophila* heads with neuronal knockdown of *Kdm5* (Figure 4G). Moreover, RPGs were dysregulated to similar degrees in human and *Drosophila* neurons, reinforcing the notion that regulating the expression of RPGs is a conserved function of KDM5C and KDM5 (Figure 4H).

To test whether reduced RPG expression in *Kdm5* knockdown neurons resulted in altered ribosome composition compared to controls, we immunoprecipitated RpL3:FLAG using anti-FLAG and carried out mass spectrometry (IP-MS) (Figure 5A). To demonstrate that whole ribosomes were recovered through immunoprecipitation of the large ribosomal subunit RPL3 prior to mass spectrometry, we confirmed the presence of the small ribosomal protein RPS12 by western blot in *Kdm5* knockdown and control heads (Figure 5B). Of the 71 ribosomal proteins (RPs) detected across all IP-MS samples, six showed decreased ribosomal association in the context of reduced KDM5: RpLP1, RpLP2, RpL10, RpL35, RpL35A and

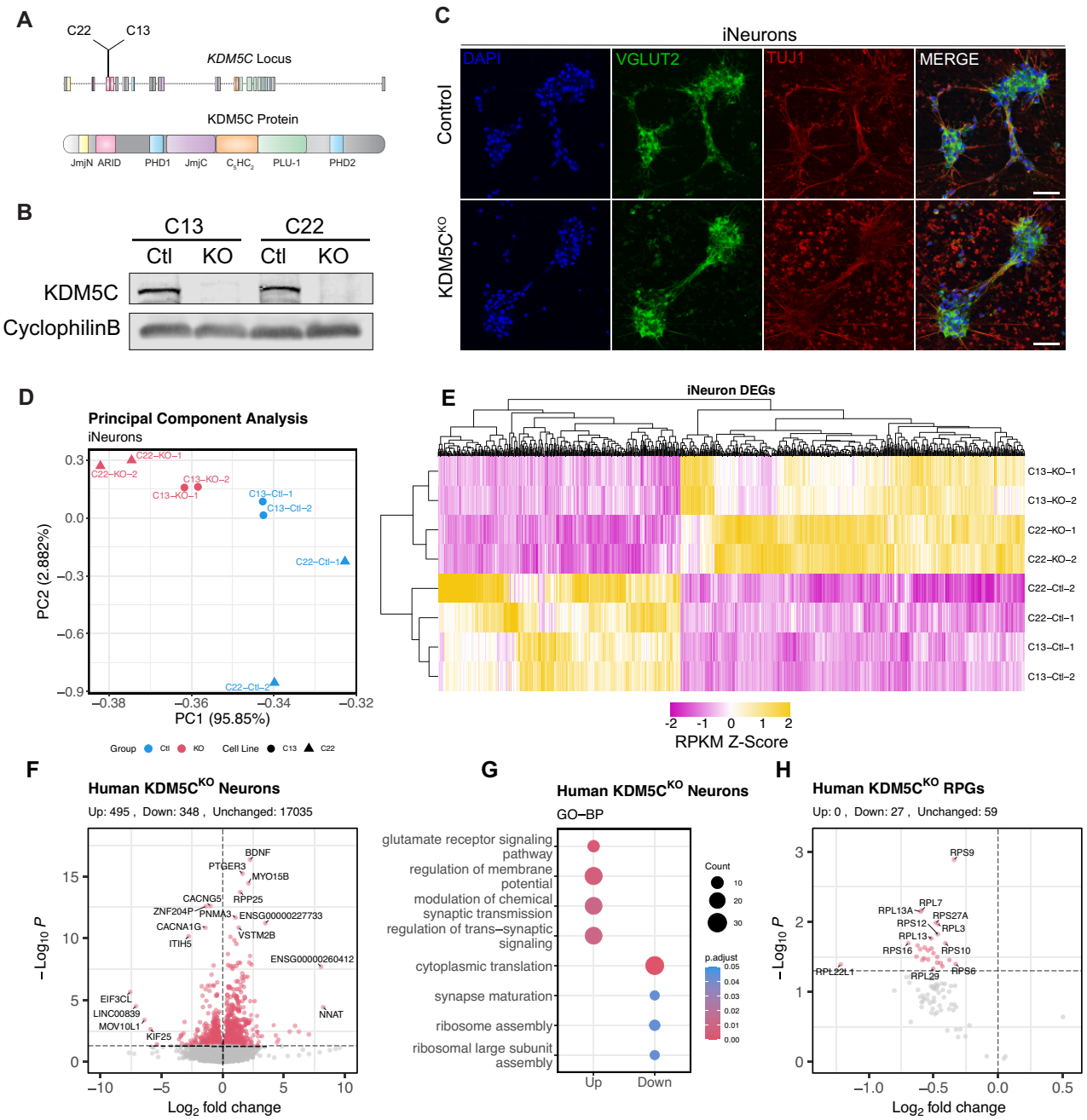

Figure 3. KDM5C is necessary for ribosomal protein gene expression in iPSC-induced glutamatergic neurons. (**A**) Schematic of *KDM5C* locus and protein. Two individual CRISPR mutants at the denoted sites induce stop codons in the *KDM5C* gene. The *KDM5C*^{C22} allele creates the change N104Vfs*33 and the *KDM5C*^{C13} allele N105Lfs*2. (**B**) Western blot of two controls and two *KDM5C*^{KO} cell lines probed with anti-KDM5C and anti-Cyclophilin B as a loading control. Both C13 and C22 lack detectable KDM5C protein. (**C**) Staining of day 21 iPSC-induced glutamatergic neurons (iNeurons) from control (upper panels; LS200C2) and *KDM5C*^{KO} (lower panels; LS200C22) stained with the DNA marker DAPI (blue), VGLUT2 (green), TUJ1 (β -TUBULIN III; red) and the merge of all channels. Scale bar represents 50 μm. (**D**) PCA analyses showing a clear clustering four control and four *KDM5C*^{KO} samples that were combined to use for RNA-seq differential expression studies. (**E**) Heatmap showing the consistency between samples of differentially expressed genes comparing control and *KDM5C*^{KO} iNeurons. Yellow: up, purple: down. (**F**) Volcano Plot of RNA-seq analysis of iNeurons comparing quadruplicate samples of *KDM5C*^{KO} and controls. (**G**) GO-BP analyses show that *KDM5C*^{KO} iNeurons show enrichment for RPGs among downregulated genes. (**H**) Volcano plot specifically showing expression of RPGs. Red indicates significantly affected using 5% FDR.

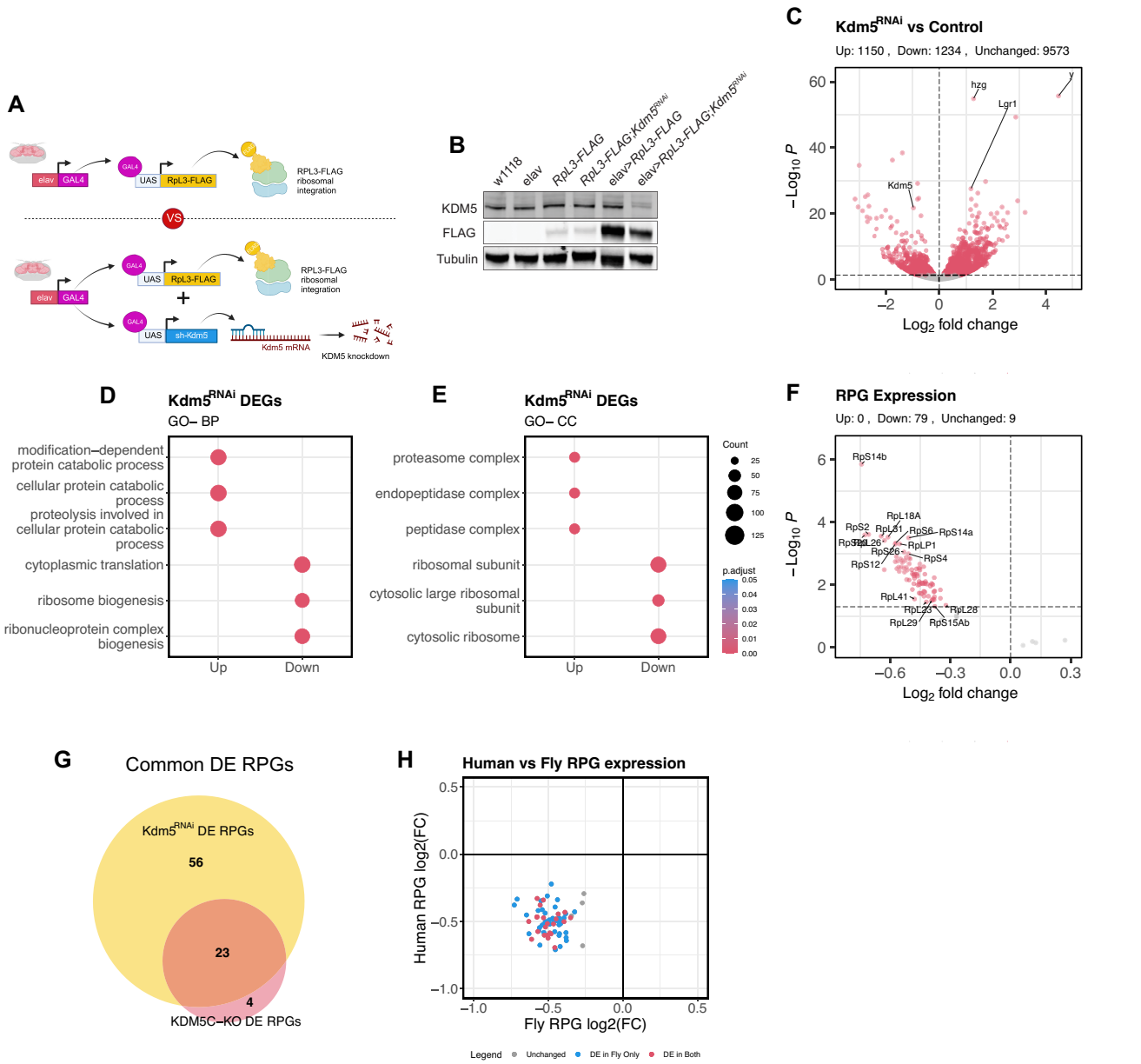

Figure 4. Neuronal knockdown of *Kdm5* results in reduced RPG expression in RpL3 overexpression background. (**A**) A schematic of the genetic strategy used to interrogate neuron-specific ribosome biology. (**B**) Western blot using anti-KDM5, anti-FLAG and anti-Tubulin (loading control) to show expression of RPL3:FLAG in the presence of the elav-GAL4 driver and reduced KDM5 only in presence of both elav-Gal4 and *Kdm5*^{RNAi}. (**C**) Volcano plot of RNA-Seq from heads of *elav-GAL4 > RPL3:FLAG; UAS-Kdm5*^{RNAi} heads compared to control animals not expressing the UAS-*Kdm5*^{RNAi}transgene. (**D**) GO-BP shows downregulated genes are enriched for ribosome related terms. (**E**) GO-CC shows downregulated genes are enriched ribosome related terms. (**F**) Volcano plot of RPGs show that majority of RPGs are downregulated when *Kdm5* is knocked down in the context of RPL3:FLAG overexpression. (**G**) 23 RPGs are commonly downregulated between human *KDM5C*^{KO} iNeurons and *Drosophila* neuronal *Kdm5*^{RNAi}. Green denotes RPG. Red denotes significantly downregulated RPG. (**H**) Scatterplot of RPGs $\log_2$ (FC) from human *KDM5C*^{KO} neurons and *Kdm5*^{RNAi} heads shows a similar degree of downregulation across species.

RpS11 (P-value < 0.05; Figure 5C; Supplementary Table S4). All six of these differentially associated RPs showed decreased mRNA levels, although many other similarly reduced RPGs did not show reduced ribosome association, suggesting that these RPs may have another layer of regulation for ribosome integration consistent with previous reports of post-transcriptional regulation (54) (Figure 5D). Overlapping gene expression information from human and *Drosophila* neurons with IP-MS data of differentially associated RPs revealed four RPs that were consistently decreased across all three experiments: RPS11, RPL10, RPLP1 and RPLP2 (Figure 5E). Interestingly, RPL10, RPLP1, RPLP2 are part of the ribosomal stalk of the human ribosome (4V6X), a key element of the ribosome that recruits translation elongation factors (Figure 5F) (55,56). Thus KDM5 is needed for proper ribosome composition and may be particularly important for ribosome stalk function.

To determine if knockdown of *Kdm5* affected the translational landscape in neurons, we performed Ribo-Seq. To do this, we used RPL3:FLAG to immunoprecipitate ribosomes,

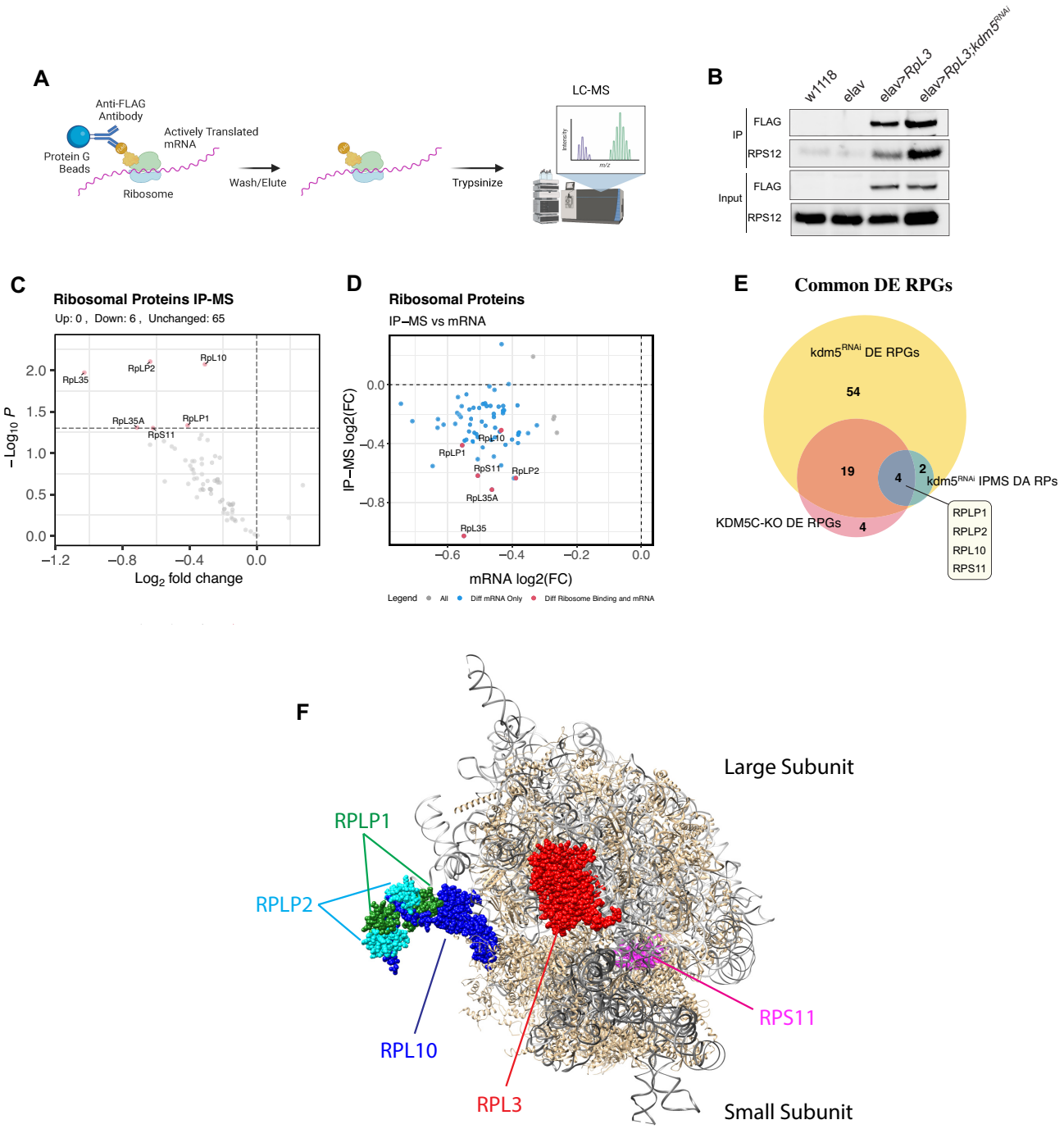

Figure 5. *Kdm5* knockdown alters ribosome composition. (**A**) Schematic of immuno-precipitation-mass spectrometry (IP-MS) experiment using RPL3:FLAG. (**B**) Western blot probed with anti-FLAG to show RPL3:FLAG and anti-RPS12 from immunoprecipitation analyses. Both large and small subunits are being recovered when using immunoprecipitating RPL3:FLAG. (**C**) Volcano plot of ribosomal proteins (RPs) show decreased ribosome-association of six RPs in *Kdm5*^{RNAi} heads. (**D**) Scatterplot comparing $\log_2$ (FC)s of all RPs from IP-MS and RNA-Seq experiments. All six RPs that show reduced ribosome association have decreased mRNA levels. (**E**) Venn diagram comparing differentially expressed (DE) RPGs from human *KDM5C*^{KO} iNeurons, DE RPGs from *Kdm5*^{RNAi} heads, and differentially associated ribosom proteins shows four commonly reduced RPs: RPL10, RPS11, RPLP1 and RPLP2. (**F**) Crystal structure of the human 80S ribosome (4v6x) with commonly dysregulated RPs highlighted. RPL3 is highlighted in red, RPS11 in magenta, RPL10 in blue, RPLP1 in green and RPLP2 in cyan.

which were treated with RNase to digest free mRNA to leave a footprint where each ribosome resides (Figure 6A) (40,52). Sequencing these 24–32 bp ribosome footprints (RFPs) allows the translation efficiency (TE) of mRNAs to be determined. To quantify the differences between control and neuronal *Kdm5* knockdown Ribo-Seq data, we used ORFik, as this tool provides a standardized, reproducible workflow and advanced analytic tools (Supplementary Table S3). (41) Consistent with our recovery of mRNAs from actively translating ribosomes, recovered RFPs were 24–33 bp in size, with a peak at 27 bp, 95% of which mapped to coding sequences (Supplementary Figure S5A-E). To achieve codon-resolution of our Ribo-Seq data, we performed p-shifting on RFPs ranging from 26 to 30 bp as they reproduced a 3nt periodicity and used these for downstream analyses.

To understand how RFP abundance related to mRNA levels for each gene, we compared the $\log_2$ (FC) of RFPs to those determined by our RNA-seq data (Figure 6B). This allowed us to assign each gene into one of four categories: 'Translation' where mRNA levels are unchanged while RFP changes, 'Buffering' where mRNA and RFP are regulated in opposite directions, 'mRNA abundance' where mRNA and RFP are regulated in the same direction, and 'No change' where there is no change to RFP or mRNA (red, blue, green, and gray, respectively, in Figure 6B, C) (41). This revealed that 1458 genes were regulated at the level of translation, 1708 genes showed buffering, and 615 genes were regulated through mRNA abundance (Figure 6B, Supplementary Figure S6A–L). Genes in all three categories can show altered TE, which is quantified by normalizing the ratio of RFPs to total mRNA (Figure 6C, Supplementary Figure S6A–R). This identified 2222 genes with significantly decreased TE in *Kdm5* knockdown neurons and 1213 with increased TE (FDR < 0.05; Figure 6C). In addition to a larger number of genes with reduced TE, the extent to which TE was altered was greater, suggesting that the primary consequence of *Kdm5* knockdown is lower levels of translation.

To understand how *Kdm5* knockdown affected ribosome function, we focused on genes in the 'Translation' category. Of the 1458 genes regulated through translation, 451 showed increased TE and 1007 were decreased (Figure 6D). Genes with increased TE showed enrichment for categories related to transport and secretion, including *Secretory 3* (*Sec3*), *Calcium-dependent secretion activator* (*Cadps*), and *Cysteine string protein* (*Csp*) (Figure 6E, F). Genes with reduced TE were enriched for those whose protein products function in mitochondrial cellular respiration, including subunits of ATP synthase and NADH dehydrogenase complexes (Figure 6E, F). To examine whether genes with decreased TE were enriched for key metabolic pathways in mitochondria, we used the KEGG database and found that oxidative phosphorylation (OXPHOS), the TCA cycle, glycolysis, and fatty acid metabolism were the most affected (Figure 6G) (57). Genes related to these processes show clear depletion of RFPs across their mRNAs in $Kdm5^{RNAi}$ animals (red compared to grey in Figure 6H–J).

Extending our Ribo-Seq analyses, we tested whether the changes to translation could be due to altered codon usage. Increased codon occupancy suggests ribosome stalling which could be due, in part, to the depletion of cognate charged tRNAs (58–60). No significant changes were observed in codon occupancy at P-sites, where the tRNA attached to the growing amino-acid chain is positioned (Supplementary Figure S7A, B). At A-sites where the amino-acyl tRNA is positioned, we found increased ribosome occupancy of Valine:GTA, Isoleucine:ATA, Arginine:AGG/AGA and Serine:TCA in *Kdm5* knockdown neurons. Conversely, we observed decreased occupancy in codons Valine:GTC, Arginine:CGG, Serine:AGC and Proline:CCC (Supplementary Figure S7C-D). With ribosome occupancy both increasing and decreasing for tRNAs bearing identical amino acids, it is possible that these data reflect codon preference. The codons with increased ribosome occupancy were not optimal or preferred, whereas those with a decreased ribosome occupancy were either optimal or preferred (Supplementary Figure S7E) (60). Thus, in $Kdm5^{RNAi}$ neurons ribosomes are more likely to be stalled at non-optimal codons encoding valine, isoleucine, serine and arginine, but are less stalled when these codons are optimal.

Loss of *Kdm5* alters mitochondrial metabolism

To understand if the decreased TE of mRNAs involved in mitochondrial metabolism affected the steady state cellular concentration of corresponding metabolites, we performed metabolomic analysis using adult heads. PCA analysis revealed a clear separation between the metabolic profiles of neuronal *Kdm5* knockdown and control animals (Figure 7A). Of the 334 metabolites identified with high confidence, 19 were significantly increased and 63 decreased in *Kdm5* knockdown animals down (Figure 7B; Supplementary Table S5). Using mRNA regulated through translation, we used MetaboAnalyst 6.0 to integrate TE and metabolite data to determine which metabolic pathways were most impacted (43,61). These included the TCA cycle, beta-alanine metabolism, purine metabolism, and arginine metabolism (Figure 7C, D). Within the glycolysis pathway key metabolites such as glucose-6-phosphate (G6P), glycerol-3-phosphate (G3P) and 3-phosphoglyceric acid (3PG) were reduced (Figure 7E). There was also a general downregulation of TCA cycle metabolites that correlated with reduced RFPs from mRNAs encoding enzymes required for progression through the TCA cycle (Figure 7F; Supplementary Figure S8). In contrast, Fatty acids (FAs) were generally increased in the $Kdm5^{RNAi}$ compared to controls, particularly C5 and C12-C18 FAs (Figure 7G). mRNA encoding for proteins responsible for lipid biosynthesis and oxidation also showed a decreased TE (Supplementary Figure S9). Together, these data suggest an overall lowering of TCA activity in neuronal mitochondria.

Glycolysis and the TCA cycle are interwoven with amino acid metabolism, redox status, and energy status of the cell. The switch in A-site codon occupancy from non-optimal to optimal codons encoding the same amino acid in *Kdm5* knockdown neurons suggests a potential change to amino acid levels. Integrated pathway analysis suggested that alanine, arginine, and proline metabolism were affected (Figure 7C). Examining the levels of amino acids and their derivatives detected in our metabolomic study, no changes were detected in levels of isoleucine, valine, arginine, or proline, although the arginine precursor citrulline, a key metabolite in the urea cycle, was decreased (Figure 7H). Alanine, leucine, and lysine were all reduced in neuronal *Kdm5* knockdown heads compared to control. Serine and its derivative O-phospho-L-serine were slightly ($P = 0.09$), or significantly reduced,

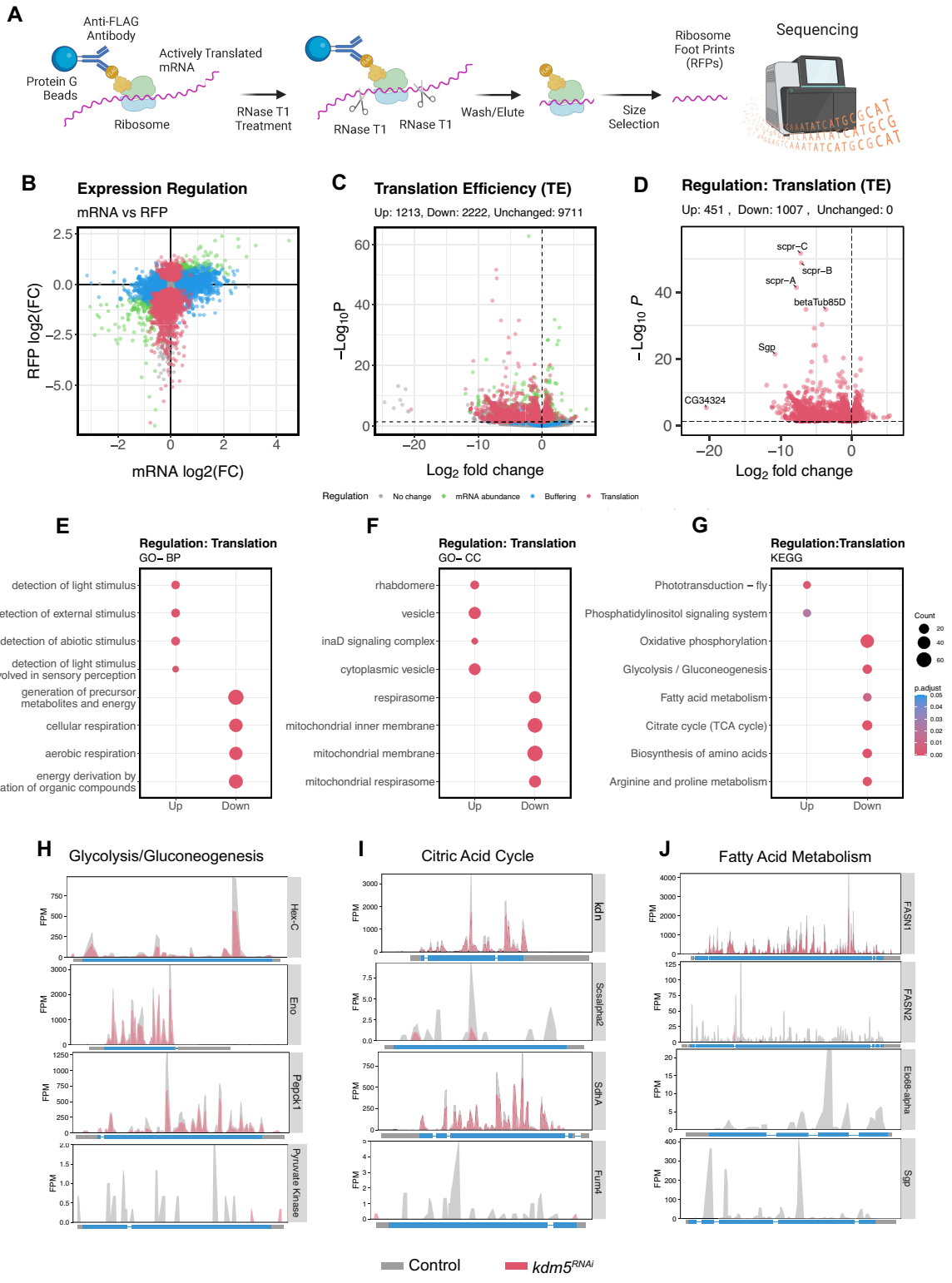

Figure 6. Neuronal *Kdm5* knockdown reduces translation efficiency of mRNAs related to mitochondrial metabolism. (**A**) Schematic of the Ribo-Seq experiment performed using adult *Drosophila* heads. (**B**) Scatterplot of $\log_2$ (FC)s of ribosome footprints (RFPs) and mRNA. Regulation of transcripts categorized by Translation in red, Buffering in blue, and mRNA abundance in green, and no change in gray. There is a large downregulation of RFPs in $Kdm5^{RNAi}$ neurons compared to control. (**C**) Volcano plot of translation efficiency (TE) of each gene categorized by regulation. There is a large downregulation of TE in $Kdm5^{RNAi}$ neurons compared to control. (**D**) Volcano Plot of translation efficiency (TE) of mRNA regulated through translation. (**E**) GO-BP of mRNA regulated through translation. Downregulated mRNAs are enriched for terms associated with respiration. (**F**) GO-CC of mRNA regulated through translation. Downregulated mRNAs were enriched for terms associated with mitochondria, while upregulated mRNAs were associated with vesicles and trafficking. (**G**) KEGG Ontology mRNA regulated through translation. Downregulated mRNA are enriched for terms associated with mitochondrial metabolism. (**H**) RFP tracings of mRNA encoding for proteins in glycolysis pathway. Control is in gray and $Kdm5^{RNAi}$ in red (also in I, J). (**I**) RFP tracings of mRNA encoding for proteins in the tricarboxylic acid (TCA) cycle. (**J**) RFP tracings of mRNA encoding for proteins in fatty acid metabolism pathways.

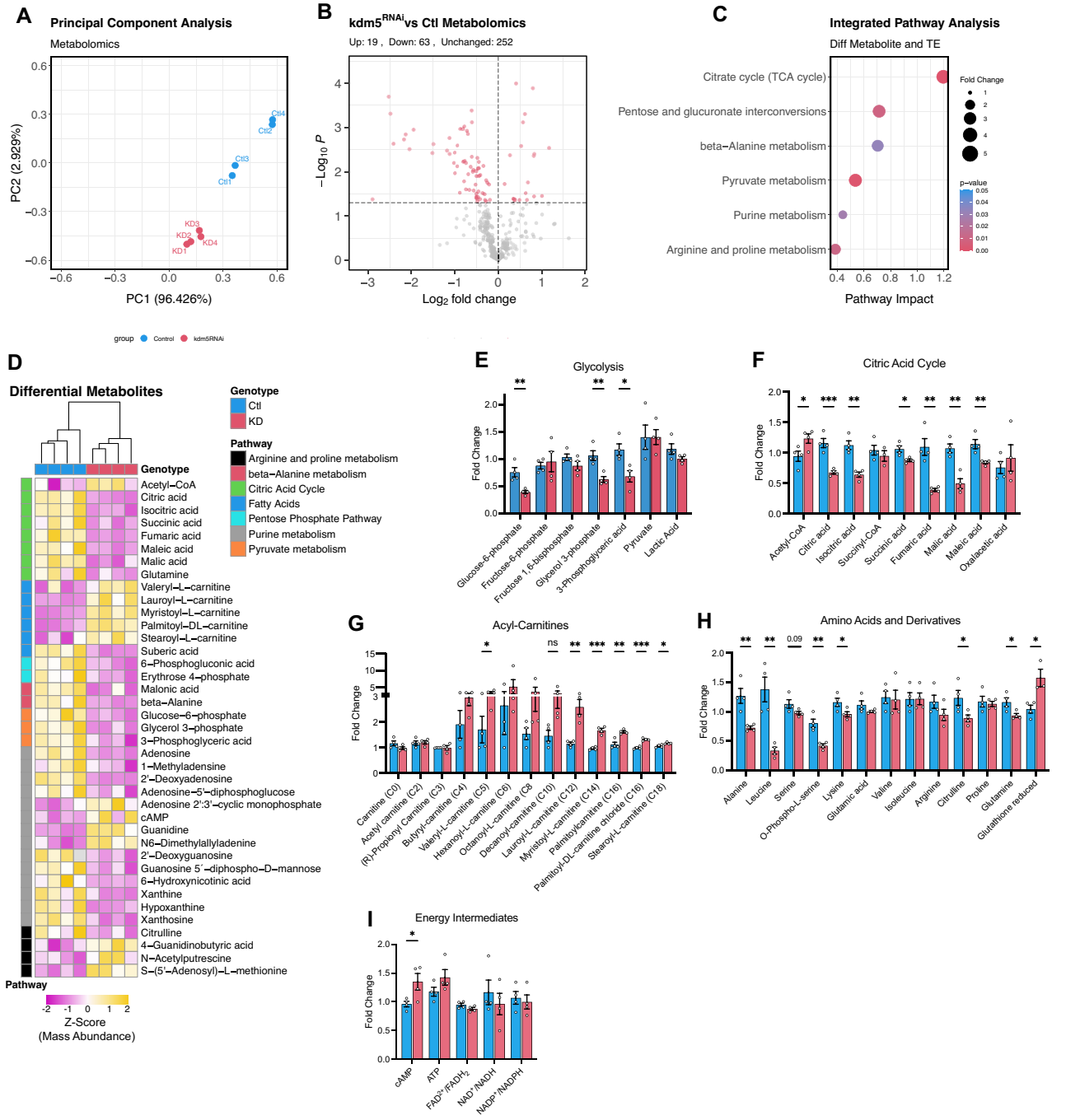

Figure 7. Loss of KDM5 affects the neuronal metabolome. (**A**) PCA of metabolomic data shows a clear separation between elav-GAL4, UAS-*Kdm5*^{RNAi} (elav > *Kdm5*^{RNAi}) (red) neurons compared to control (blue). (**B**) Volcano plot of detected metabolites. Red indicates significantly altered ($P < 0.05$). (**C**) Integrated pathway analysis revealed pathways in which both Ribo-Seq and metabolomic data contribute to changes. Fold change and *P*-value are indicated by size and color, respectively. (**D**) Heatmap showing *Z*-scores of mass abundances of metabolites found in enriched pathways found in (C). (**E**) Metabolites of the glycolysis pathway with control shown in blue and elav > *Kdm5*^{RNAi} in red. For D–H, data shown are changes of mass abundances normalized to a single control sample. (**F**) Metabolites of the citric acid cycle are generally decreased in elav > *Kdm5*^{RNAi} neurons compared to control. (**G**) Metabolites of fatty acids show an increase in long chain fatty acid in elav > *Kdm5*^{RNAi} heads compared to control. (**H**) Amino acid levels in elav > *Kdm5*^{RNAi} heads compared to control. (**I**) Quantification of energy intermediates shows that they are unchanged except for cAMP which is upregulated in elav > *Kdm5*^{RNAi} heads compared to control. Two-sided Student's *t*-test. *P*-values *<0.05, **<0.01, ***<0.001, ****<0.0001.

respectively (Figure 7H). Glutamine metabolites were also slightly affected, with glutamine itself being slightly decreased and reduced glutathione increased. Whether these subtle changes affect neuronal signaling or redox state is not clear. Interestingly, despite these changes to mitochondrial energy pathways, there was no change to ATP, $FAD^{2+}/FADH_2$, $NAD^+/NADH$, or $NADP^+/NADPH$ ratios suggesting compensation of other pathways or non-neuronal cell types such as glia (Figure 7I). However, cAMP was significantly elevated, supporting the view that *Kdm5* knockdown may result in cells and/or mitochondria being metabolically stressed. It should, however, be noted that steady-state levels of metabolites do not necessarily reflect metabolic flux through mitochondrial pathways or oxygen consumption, and the extent to which loss of *Kdm5* affects these remains an open question. Overall, these data link KDM5-regulated transcriptional programs to neuronal ribosome composition and the translation of proteins needed for proper mitochondrial and amino acid metabolism.

Discussion

Here, we use *Drosophila* and human cell models to gain insights into the basis of neurodevelopmental disorders caused by variants in *KDM5* family genes, particularly those in *KDM5C* that are associated with Claes–Jensen syndrome. Coupled with our prior analyses of the adult neuronal phenotypes of $Kdm5^{A512P}$, our analyses of five additional patient-associated missense variants show that ID-variant flies show phenotypes that are consistent with their identification in individuals with Claes–Jensen syndrome (13). These include changes to short- and/or long-term associative learning and memory, ID-relevant habituation learning, axonal growth and guidance, seizure susceptibility, and locomotion. Importantly, we find that the transcriptional changes caused by ID-associated alleles show a striking trend of altering genes associated with translation, particularly RPGs. A similar gene expression signature was observed in human $KDM5C^{KO}$ iNeurons, in keeping with the regulation of RPGs being a conserved function of KDM5 proteins. Analyses of the downstream consequences to translation revealed a strong effect on mRNAs encoding proteins required within mitochondria. This coincided with changes to mitochondrial metabolism, as exhibited by alterations in the metabolome which included lowered steady state levels of TCA cycle intermediates and altered levels of fatty acids. Together, our studies greatly extend our understanding of how KDM5 family proteins function in the brain and suggest that altered translation may play a key role in cognitive (dys)function observed in patients with ID.

Individuals with Claes–Jensen syndrome present with a broad range of features. While hemizygous males consistently show some level of intellectual disability, seizures, aggression, speech impairment, autism, and/or short stature have all additionally been reported to varying degrees (4,7). Although differences in genetic backgrounds across families is likely to contribute to this phenotypic variability, our studies using isogenic *Drosophila* strains suggest that it may be a feature of KDM5. For example, 10–35% of $Kdm5^{A224T}$, $Kdm5^{D234G}$, $Kdm5^{L854F}$, $Kdm5^{R87W}$ and $Kdm5^{Y874C}$ animals showed defective axonal growth and guidance of the mushroom body neurons, while the remaining animals showed typical neuromorphological development. It is also notable that the low frequency of these gross architectural phenotypes suggest that they are unlikely to contribute significantly to the learning and memory deficits observed in ID-variant fly strains. This is consistent with our previous observations that the $Kdm5^{A512P}$ and $Kdm5^{JmjC*}$ alleles had no morphological defects but did alter learning and/or memory (13). Altered neuronal function, similar to the excitatory synaptic activity that we have shown to be reduced at the larval neuromuscular junction, may therefore contribute to the phenotypes observed in ID-variant adult flies (12).

Despite an emphasis on altered H3K4me3 in the pathogenesis of Claes-Jensen syndrome, four of the six alleles examined here and previously do not appreciably alter this aspect of KDM5 activity (13). Although ID-alleles show disparate effects on enzymatic function, they all showed downregulation of genes required for cytoplasmic translation. This suggests that more than one activity of KDM5 contributes to its regulation of RPGs. For example, variants that do not alter enzymatic function may affect protein–protein interactions that are critical for KDM5 function. It is also notable that the regulation of this class of gene by KDM5 appears to occur primarily in neurons. In *Drosophila*, our previous analyses of epithelial wing imaginal discs did not reveal changes to RPGs (62). Similarly, while we observe changes to RPGs in $KDM5C^{KO}$ iNeurons, this has not been seen in prior studies of a range of non-neuronal mammalian cells with altered *KDM5A*, *KDM5B* or *KDM5C* (62–66). How broadly KDM5 regulates RPGs across cell types remains an open and important question. Based on the association between genetic variants in *KDM5A* and *KDM5B* and ID, it will also be interesting to determine whether these paralogs regulate RPGs in iNeurons in a similar manner to KDM5C, as this could indicate a shared pathomechanism.

Our data show that *Kdm5* knockdown in neurons led to reduced expression of RPGs, altered ribosome composition, and an overall dampening of translation. Since long-term potentiation of memory relies on *de novo* translation, our data are consistent with the hypothesis that KDM5-mediated control of RPGs contributes to the long-term memory defects observed in flies. Consistent with this, $Kdm5^{A224T}$, $Kdm5^{D234G}$, $Kdm5^{JmjC*}$ and $Kdm5^{L854F}$ show long-term memory defects and these genotypes display the most consistent and broad down regulation of RPGs. Long term potentiation of memory relies, in part, on the ability for ribosomes and mRNA to be properly trafficked to distal compartments such as dendrites and axon terminals for the development and maintenance of synapses (67–69). Our data also point to a particularly important role for the ribosomal stalk proteins RPL10, RPLP1 and RPLP2. Proteins that comprise the stalk region of the ribosome bind to, and stabilize, translation elongation factors, suggesting that their loss would result in unproductive translation and reduced TE (56). Since mRNA encoding mitochondrial proteins were most dysregulated, it is possible that these changes occur primarily in more distal neuronal compartments (70–72). Consistent with this, mRNAs encoding for RPLP1, RPLP2, RPL10 are enriched in dendrites compared to soma in rat hippocampal neurons, where they undergo dynamic incorporation into ribosomes (73). Like Claes-Jensen syndrome, dysfunction of RPL10 results in an X-linked neurodevelopmental disorder with overlapping phenotypes such as ID, seizures, and microcephaly (74). RPLP1 is also necessary for nervous system development in mice, and its deletion results in microcephaly (75). The extent to which phenotypes caused by reduced RP function overlap with KDM5 ID-variant phenotypes is unclear, and how their reduction

affects ribosome and translation localization should be explored in future studies.

Reduced levels of KDM5 in neurons had a disproportionately large effect on the translation of mRNA encoding metabolic proteins necessary for mitochondrial function (76). Prior studies of non-neuronal cell types in mammals and *Drosophila* have observed that KDM5 family proteins can directly activate or repress the expression of genes encoding mitochondrial-related proteins such as components of cytochrome C oxidase, ATP synthase complex, and mitochondrial translation in a context dependent manner (65,66,77–79). We did we not observe altered expression of this group of mitochondrial genes in ID-variants, consistent with KDM5 affecting mitochondrial function through a distinct mechanism in neurons. Our work therefore bridges an important gap between understanding conserved KDM5-directed expression programs at the levels of both transcription and translation and provides insights into the complexities of Claes–Jensen syndrome. Moreover, our data suggest a model in which *KDM5*-associated ID may be part of a broader category of disorders that show altered neuronal translation and mitochondrial function.

Data availability

Drosophila RNA-seq and Ribo-Seq fastq files have been uploaded to GEO with the accession number GSE245380. Human glutamatergic neuron data are available using GSE245515. A list of differentially expressed genes (and $\log_2$ fold change) observed in *Drosophila* ID-variants and human glutamatergic neurons compared to respective controls are provided in Supplementary Tables S1 and S2. Ribo-Seq data of differentially regulated genes are provided in Supplementary Table S3. Ribosome IP-MS data are publicly available through ProteomeXchange (project PXD046963) and are provided in Supplementary Table S4. Metabolomic data are provided in Supplementary Table S5.

Supplementary data

Supplementary Data are available at NAR Online.

Acknowledgements

We thank Nicholas Baker, Melissa Castiglione, Richard Daniel Kelly IV, Amira Millette, and members of the Einstein Intellectual and Developmental Disabilities Research Center (IDDRC) for their support and feedback throughout this project and suggestions on the manuscript. We appreciate the availability of fly strains from the Bloomington *Drosophila* Stock Center (NIH P400D018537) and antibody from Shigeki Iwase (anti-KDM5C; University of Michigan) and the Developmental Studies Hybridoma bank, created by the NICHD of the NIH and maintained at The University of Iowa. We also thank the Analytical Imaging (shared instrument grant 1S10OD023591), Flow Cytometry and Genomics core facilities at Einstein and the Einstein Cancer Center Support Grant (P30 CA013330). The stable Isotope and Metabolomics Core Facility of the Diabetes Research and Training Center (DRTC) of the Albert Einstein College of Medicine is supported by NIH/NCI grant P60DK020541.

Author contributions: Conceptualization, M.Y., H.A.M.H., B.K.T., L.E.R.B., M.F., A.S., H.M.L., J.S.; Methodology M.Y., H.A.M.H., E.P., B.K.T., A.A.S., A.L.E.R.B., M.F., X.Y.Z., S.S., H.M.L., D.Z.; Investigation, M.Y., H.A.M.H., B.K.T., A.A.S., S.S., A.S. L.E.R.B., M.F., X.Y.Z., E.P., H.M.L., D.Z and J.S.; Writing – original draft, M.Y., A.S., H.L., L.E.R.B., M.F. and J.S., Writing – Reviewing and Editing, M.Y., H.A.M.H., B.K.T., A.A.S., S.S., A.S., L.E.R.B., H.M.L., M.F, J.S.; Funding acquisition, M.Y., H.A.M.H., S.S., A.S., H.L., D.Z. and J.S., Supervision, H.M.L., A.S., D.Z. and J.S.

Funding

National Institutes of Health [T32GM149364 to M.Y. and H.A.M.H., F31GM146347 to M.Y., F31NS110278 to H.A.M.H., K12GM102779 to B.K.T., R01112783 to J.S., and P50HD105352 to J.S., D.Z. and H.M.L.]; Irma T. Hirschl Trust (to J.S.); Junior Investigator in Neuroscience Research Award from the Dominick P. Purpura Department of Neuroscience (to H.A.M.H.); Sidoli lab gratefully acknowledges for financial support from the American Federation for Aging Research (AFAR; Sagol Network GerOmics award), Deerfield (Xseed award), Relay Therapeutics, Merck, and the NIH Office of the Director [1-S10-OD030286-01]; Schenck lab was supported by the Dutch Research Council (NWO) [ZonMw Vici grant no. 09150181910022 to A.S.]; Australian National Health and Medical Research Council to the Centre for Research Excellence in Neurocognitive Disorders (CRENCD) [APP1117394]; M.F. was further supported by a grant from the Czech Science Foundation [23-07810S]; EMBO Installation grant [IG-5310-2023]. Funding for open access charge: NIH [R01112783].

Conflict of interest statement

Julie Secombe is the Chair of the Scientific Advisory Board for the KDM5C Advocacy, Research, Education, & Support (KARES) Foundation (volunteer position).

References

1. Pavlenko,E., Ruengeler,T., Engel,P. and Poepsel,S. (2022) Functions and interactions of mammalian KDM5 demethylases. *Front. Genet.*, **13**, 906662.
2. Garzón-Porras,A.M., Chory,E. and Gryder,B.E. (2023) Dynamic opposition of histone modifications. *ACS Chem. Biol.*, **18**, 1027–1036.
3. Harrington,J., Wheway,G., Willaime-Morawek,S., Gibson,J. and Walters,Z.S. (2022) Pathogenic KDM5B variants in the context of developmental disorders. *Biochim. Biophys Acta Gene Regul. Mech.*, **1865**, 194848.
4. Hatch,H.A.M. and Secombe,J. (2021) Molecular and cellular events linking variants in the histone demethylase KDM5C to the intellectual disability disorder Claes-Jensen syndrome. *FEBS J.*, **289**, 7776–7787.
5. Vallianatos,C.N. and Iwase,S. (2015) Disrupted intricacy of histone H3K4 methylation in neurodevelopmental disorders. *Epigenomics*, **7**, 503–519.
6. Leonardi,E., Aspromonte,M.C., Drongitis,D., Bettella,E., Verrillo,L., Polli,R., McEntagart,M., Licchetta,L., Dilena,R., D'Arrigo,S., *et al.* (2022) Expanding the genetics and phenotypic spectrum of lysine-specific demethylase 5C (KDM5C): A report of 13 novel variants. *Eur. J. Hum. Genet.*, **31**, 202–215.
7. Carmignac,V., Nambot,S., Lehalle,D., Callier,P., Moortgat,S., Benoit,V., Ghoumid,J., Delobel,B., Smol,T., Thuillier,C., *et al.* (2020) Further delineation of the female phenotype with KDM5C

disease causing variants: 19 new individuals and review of the literature. *Clin. Genet.*, **98**, 43–55.
8. Iwase,S., Brookes,E., Agarwal,S., Badeaux,A.I., Ito,H., Vallianatos,C.N., Tomassy,G.S., Kasza,T., Lin,G., Thompson,A., *et al.* (2016) A mouse model of X-linked intellectual disability associated with impaired removal of histone methylation. *Cell Rep.*, **14**, 1000–1009.
9. Scandaglia,M., Lopez-Atalaya,J.P., Medrano-Fernandez,A., Lopez-Cascales,M.T., Del Blanco,B., Lipinski,M., Benito,E., Olivares,R., Iwase,S., Shi,Y, *et al.* (2017) Loss of Kdm5c causes spurious transcription and prevents the fine-tuning of activity-regulated enhancers in neurons. *Cell Rep.*, **21**, 47–59.
10. Vallianatos,C.N., Raines,B., Porter,R.S., Bonefas,K.M., Wu,M.C., Garay,P.M., Collette,K.M., Seo,Y.A., Dou,Y., Keegan,C.E., *et al.* (2020) Mutually suppressive roles of KMT2A and KDM5C in behaviour, neuronal structure, and histone H3K4 methylation. *Commun. Biol.*, **3**, 278.
11. El Hayek,L., Tuncay,I.O., Nijem,N., Russell,J., Ludwig,S., Kaur,K., Li,X., Anderton,P., Tang,M., Gerard,A., *et al.* (2020) KDM5A mutations identified in autism spectrum disorder using forward genetics. *eLife*, **9**, e56883.
12. Belalcazar,H.M., Hendricks,E.L., Zamurrad,S., Liebl,F.L.W. and Secombe,J. (2021) The histone demethylase KDM5 is required for synaptic structure and function at the Drosophila neuromuscular junction. *Cell Rep.*, **34**, 108753.
13. Zamurrad,S., Hatch,H.A.M., Drelon,C., Belalcazar,H.M. and Secombe,J. (2018) A Drosophila model of intellectual disability caused by mutations in the histone demethylase KDM5. *Cell Rep.*, **22**, 2359–2369.
14. Ford,T.J.L., Jeon,B.T., Lee,H. and Kim,W.Y. (2022) Dendritic spine and synapse pathology in chromatin modifier-associated autism spectrum disorders and intellectual disability. *Front. Mol. Neurosci.*, **15**, 1048713.
15. Exposito-Alonso,D. and Rico,B. (2022) Mechanisms underlying circuit dysfunction in neurodevelopmental disorders. *Annu. Rev. Genet.*, **56**, 391–422.
16. Iwase,S., Lan,F., Bayliss,P., De La Torre-Ubieta,L., Huarte,M., Qi,H.H., Whetstine,R., Johnathan,Bonni, A., Roberts,T.M. and Shi,Y. (2007) The X-linked mental retardation gene SMCX/JARID1C defines a family of histone H3 lysine 4 demethylases. *Cell*, **128**, 1077–1088.
17. Lussi,Y.C., Mariani,L., Friis,C., Peltonen,J., Myers,T.R., Krag,C., Wong,G. and Salcini,A.E. (2016) Impaired removal of H3K4 methylation affects cell fate determination and gene transcription. *Development*, **143**, 3751–3762.
18. Mariani,L., Lussi,Y.C., Vandamme,J., Riveiro,A. and Salcini,A.E. (2016) The H3K4me3/2 histone demethylase RBR-2 controls axon guidance by repressing the actin-remodeling gene wsp-1. *Development*, **143**, 851–863.
19. Hatch,H.A.M., Belalcazar,H.M., Marshall,O.J. and Secombe,J. (2021) A KDM5-Prospero transcriptional axis functions during early neurodevelopment to regulate mushroom body formation. *eLife*, **10**, e63886.
20. Holt,C.E., Martin,K.C. and Schuman,E.M. (2019) Local translation in neurons: visualization and function. *Nat. Struct. Mol. Biol.*, **26**, 557–566.
21. Mila,M., Alvarez-Mora,M.I., Madrigal,I. and Rodriguez-Revenga,L. (2018) Fragile X syndrome: An overview and update of the FMR1 gene. *Clin. Genet.*, **93**, 197–205.
22. Dockendorff,T.C. and Labrador,M. (2018) The fragile X protein and genome function. *Mol. Neurobiol.*, **56**, 711–721.
23. Drelon,C., Belalcazar,H.M. and Secombe,J. (2018) The histone demethylase KDM5 is essential for larval growth in Drosophila. *Genetics*, **209**, 773–787.
24. Navarro-Costa,P., McCarthy,A., Prudencio,P., Greer,C., Guilgur,L.G., Becker,J.D., Secombe,J., Rangan,P. and Martinho,R.G. (2016) Early programming of the oocyte epigenome temporally controls late prophase I transcription and chromatin remodelling. *Nat. Commun.*, **7**, 12331.
25. Bischof,J., Maeda,R.K., Hediger,M., Karch,F. and Basler,K. (2007) An optimized transgenesis system for Drosophila using germ-line-specific phiC31 integrases. *Proc. Natl. Acad. Sci. U.S.A.*, **104**, 3312–3317.
26. Barnes,J., Salas,F., Mokhtari,R., Dolstra,H., Pedrosa,E. and Lachman,H.M. (2018) Modeling the neuropsychiatric manifestations of Lowe syndrome using induced pluripotent stem cells: defective F-actin polymerization and WAVE-1 expression in neuronal cells. *Mol. Autism*, **9**, 44.
27. Zhang,Y., Pak,C., Han,Y., Ahlenius,H., Zhang,Z., Chanda,S., Marro,S., Patzke,C., Acuna,C., Covy,J., *et al.* (2013) Rapid single-step induction of functional neurons from human pluripotent stem cells. *Neuron*, **78**, 785–798.
28. Ji,Z., Kiparaki,M., Folgado,V., Kumar,A., Blanco,J., Rimesso,G., Chuen,J., Liu,Y., Zheng,D. and Baker,N.E. (2019) Drosophila RpS12 controls translation, growth, and cell competition through Xrp1. *PLoS Genet.*, **15**, e1008513.
29. Schneider,C.A., Rasband,W.S. and Eliceiri,K.W. (2012) NIH Image to ImageJ: 25 years of image analysis. *Nat. Methods*, **9**, 671–675.
30. Trannoy,S., Redt-Clouet,C., Dura,J.M. and Preat,T. (2011) Parallel processing of appetitive short- and long-term memories in Drosophila. *Curr. Biol.*, **21**, 1647–1653.
31. Fenckova,M., Blok,L.E.R., Asztalos,L., Goodman,D.P., Cizek,P., Singgih,E.L., Glennon,J.C., IntHout,J., Zweier,C., Eichler,E.E., *et al.* (2019) Habituation learning is a widely affected mechanism in Drosophila models of intellectual disability and autism spectrum disorders. *Biol. Psychiatry*, **86**, 294–305.
32. Mituzaite,J., Petersen,R., Claridge-Chang,A. and Baines,R.A. (2021) Characterization of seizure induction methods in*Drosophila*. *Eneuro*, **8**, ENEURO.0079-0021.
33. Fischer,F.P., Karge,R.A., Weber,Y.G., Koch,H., Wolking,S. and Voigt,A. (2023) Drosophila melanogaster as a versatile model organism to study genetic epilepsies: an overview. *Front Mol. Neurosci.*, **16**, 1116000.
34. Mi,K., Li,Y., Yang,Y., Secombe,J. and Liu,X. (2023) DVT: a high-throughput analysis pipeline for locomotion and social behavior in adult Drosophila melanogaster. *Cell Biosci.*, **13**, 187.
35. Yamanaka,O. and Takeuchi,R. (2018) UMATracker: an intuitive image-based tracking platform. *J. Exp. Biol.*, **16**, 221.
36. Love,M.I., Huber,W. and Anders,S. (2014) Moderated estimation of fold change and dispersion for RNA-seq data with DESeq2. *Genome Biol.*, **15**, 550.
37. Dobin,A., Davis,C.A., Schlesinger,F., Drenkow,J., Zaleski,C., Jha,S., Batut,P., Chaisson,M. and Gingeras,T.R. (2013) STAR: ultrafast universal RNA-seq aligner. *Bioinformatics*, **29**, 15–21.
38. Harrow,J., Frankish,A., Gonzalez,J.M., Tapanari,E., Diekhans,M., Kokocinski,F., Aken,B.L., Barrell,D., Zadissa,A., Searle,S., *et al.* (2012) GENCODE: the reference human genome annotation for The ENCODE Project. *Genome Res.*, **22**, 1760–1774.
39. Li,B. and Dewey,C.N. (2011) RSEM: accurate transcript quantification from RNA-Seq data with or without a reference genome. *BMC Bioinf.*, **12**, 323.
40. Chen,X. and Dickman,D. (2021) Tissue-specific ribosome profiling in Drosophila. *Methods Mol. Biol.*, **2252**, 175–188.
41. Tjeldnes,H., Labun,K., Torres Cleuren,Y., Chyzynska,K., Swirski,M. and Valen,E. (2021) ORFik: a comprehensive R toolkit for the analysis of translation. *BMC Bioinf.*, **22**, 336.
42. Aguilan,J.T., Kulej,K. and Sidoli,S. (2020) Guide for protein fold change and p-value calculation for non-experts in proteomics. *Mol. Omics*, **16**, 573–582.
43. Pang,Z., Zhou,G., Ewald,J., Chang,L., Hacariz,O., Basu,N. and Xia,J. (2022) Using MetaboAnalyst 5.0 for LC-HRMS spectra processing, multi-omics integration and covariate adjustment of global metabolomics data. *Nat. Protoc.*, **17**, 1735–1761.
44. Jensen,L.R., Amende,M., Gurok,U., Moser,B., Gimmel,V., Tzschach,A., Janecke,A.R., Tariverdian,G., Chelly,J., Fryns,J.P., *et al.* (2005) Mutations in the JARID1C gene, which is involved in transcriptional regulation and chromatin remodeling, cause X-linked mental retardation. *Am. J. Hum. Genet.*, **76**, 227–236.

45. Abidi,F.E., Holloway,L., Moore,C.A., Weaver,D.D., Simensen,R.J., Stevenson,R.E., Rogers,R.C. and Schwartz,C.E. (2008) Mutations in JARID1C are associated with X-linked mental retardation, short stature and hyperreflexia. *J. Med. Genet.*, **45**, 787–793.
46. Tzschach,A., Lenzner,S., Moser,B., Reinhardt,R., Chelly,J., Fryns,J.P., Kleefstra,T., Raynaud,M., Turner,G., Ropers,H.H., *et al.* (2006) Novel JARID1C/SMCX mutations in patients with X-linked mental retardation. *Hum. Mutat.*, **27**, 389.
47. Li,L., Greer,C., Eisenman,R.N. and Secombe,J. (2010) Essential functions of the histone demethylase lid. *PLoS Genet.*, **6**, e1001221.
48. Blok,L.E.R., Boon,M., van Reijmersdal,B., Hoffler,K.D., Fenckova,M. and Schenck,A. (2022) Genetics, molecular control and clinical relevance of habituation learning. *Neurosci. Biobehav. Rev.*, **143**, 104883.
49. Vivanti,G., Hocking,D.R., Fanning,P.A.J., Uljarevic,M., Postorino,V., Mazzone,L. and Dissanayake,C. (2018) Attention to novelty versus repetition: contrasting habituation profiles in Autism and Williams syndrome. *Dev. Cogn. Neurosci.*, **29**, 54–60.
50. Ethridge,L.E., White,S.P., Mosconi,M.W., Wang,J., Byerly,M.J. and Sweeney,J.A. (2016) Reduced habituation of auditory evoked potentials indicate cortical hyper-excitability in fragile X syndrome. *Translational Psychiatry*, **6**, e787.
51. Liu,X. and Secombe,J. (2015) The histone demethylase KDM5 activates gene expression by recognizing chromatin context through its PHD reader motif. *Cell Rep.*, **13**, 2219–2231.
52. Chen,X. and Dickman,D. (2017) Development of a tissue-specific ribosome profiling approach in Drosophila enables genome-wide evaluation of translational adaptations. *PLoS Genet.*, **13**, e1007117.
53. Eissenberg,J.C., Lee,M.G., Schneider,J., Ilvarsonn,A., Shiekhattar,R. and Shilatifard,A. (2007) The trithorax-group gene in Drosophila little imaginal discs encodes a trimethylated histone H3 Lys4 demethylase. *Nat. Struct. Mol. Biol.*, **14**, 344–346.
54. Sidhaye,J., Trepte,P., Sepke,N., Novatchkova,M., Schutzbier,M., Dürnberger,G., Mechtler,K. and Knoblich,J.A. (2023) Integrated transcriptome and proteome analysis reveals posttranscriptional regulation of ribosomal genes in human brain organoids. *eLife*, **12**, e85135.
55. Anger,A.M., Armache,J.-P., Berninghausen,O., Habeck,M., Subklewe,M., Wilson,D.N. and Beckmann,R. (2013) Structures of the human and Drosophila 80S ribosome. *Nature*, **497**, 80–85.
56. Wahl,M.C. and Möller,W. (2002) Structure and function of the acidic ribosomal stalk proteins. *Curr Protein Pept Sci.*, **3**, 93–106.
57. Kanehisa,M. and Goto,S. (2000) KEGG: kyoto encyclopedia of genes and genomes. *Nucleic Acids Res.*, **28**, 27–30.
58. Barrington,C.L., Koch,A.L., Galindo,G., Larkin-Gero,E., Morrison,E.J., Tisa,S., Stasevich,T.J. and Rissland,O.S. (2023) Synonymous codon usage regulates translation initiation. *Cell Rep.*, **42**, 113413.
59. Rubio,A., Ghosh,S., Mülleder,M., Ralser,M. and Mata,J. (2021) Ribosome profiling reveals ribosome stalling on tryptophan codons and ribosome queuing upon oxidative stress in fission yeast. *Nucleic Acids Res.*, **49**, 383–399.
60. Vicario,S., Moriyama,E.N. and Powell,J.R. (2007) Codon usage in twelve species of Drosophila. *BMC Evol. Biol.*, **7**, 226.
61. Xia,J., Psychogios,N., Young,N. and Wishart,D.S. (2009) MetaboAnalyst: a web server for metabolomic data analysis and interpretation. *Nucleic Acids Res.*, **37**, W652–W660.
62. Drelon,C., Belalcazar,H.M. and Secombe,J. (2018) The histone demethylase KDM5 is essential for larval growth in drosophila. *Genetics*, **209**, 773–787.
63. Kidder,B.L., Hu,G. and Zhao,K. (2014) KDM5B focuses H3K4 methylation near promoters and enhancers during embryonic stem cell self-renewal and differentiation. *Genome Biol.*, **15**, R32.
64. Kirtana,R., Manna,S. and Patra,S.K. (2023) KDM5A noncanonically binds antagonists MLL1/2 to mediate gene regulation and promotes epithelial to mesenchymal transition. *Biochim. Biophys. Acta Gene Regul. Mech.*, **1866**, 194986.
65. Varaljai,R., Islam,A.B., Beshiri,M.L., Rehman,J., Lopez-Bigas,N. and Benevolenskaya,E.V. (2015) Increased mitochondrial function downstream from KDM5A histone demethylase rescues differentiation in pRB-deficient cells. *Genes Dev.*, **29**, 1817–1834.
66. Liu,H., Zhai,L., Liu,Y., Lu,D., Vander Ark,A., Yang,T. and Krawczyk,C.M. (2023) The histone demethylase KDM5C controls female bone mass by promoting energy metabolism in osteoclasts. *Sci. Adv.*, **9**, eadg0731.
67. Costa-Mattioli,M., Sossin,W.S., Klann,E. and Sonenberg,N. (2009) Translational control of long-lasting synaptic plasticity and memory. *Neuron*, **61**, 10–26.
68. Gal-Ben-Ari,S., Kenney,J.W., Ounalla-Saad,H., Taha,E., David,O., Levitan,D., Gildish,I., Panja,D., Pai,B., Wibrand,K., *et al.*(2012) Consolidation and translation regulation. *Learn Mem.*, **19**, 410–422.
69. Huber,K.M., Kayser,M.S. and Bear,M.F. (2000) Role for rapid dendritic protein synthesis in hippocampal mGluR-dependent long-term depression. **288**, 1254–1257.
70. Luan,Y., Tang,N., Yang,J., Liu,S., Cheng,C., Wang,Y., Chen,C., Guo,Y.-N., Wang,H., Zhao,W., *et al.* (2022) Deficiency of ribosomal proteins reshapes the transcriptional and translational landscape in human cells. *Nucleic Acids Res.*, **50**, 6601–6617.
71. Milenkovic,I., Santos Vieira,H.G., Lucas,M.C., Ruiz-Orera,J., Patone,G., Kesteven,S., Wu,J., Feneley,M., Espadas,G., Sabidó,E., *et al.* (2023) Dynamic interplay between RPL3- and RPL3L-containing ribosomes modulates mitochondrial activity in the mammalian heart. *Nucleic Acids Res.*, **51**, 5301–5324.
72. Shi,Z., Fujii,K., Kovary,K.M., Genuth,N.R., Röst,H.L., Teruel,M.N. and Barna,M. (2017) Heterogeneous ribosomes preferentially translate distinct subpools of mRNAs genome-wide. *Mol. Cell*, **67**, 71–83.
73. Fusco,C.M., Desch,K., Dörrbaum,A.R., Wang,M., Staab,A., Chan,I.C.W., Vail,E., Villeri,V., Langer,J.D. and Schuman,E.M. (2021) Neuronal ribosomes exhibit dynamic and context-dependent exchange of ribosomal proteins. *Nat. Commun.*, **12**, 6127.
74. Brooks,S.S., Wall,A.L., Golzio,C., Reid,D.W., Kondyles,A., Willer,J.R., Botti,C., Nicchitta,C.V., Katsanis,N. and Davis,E.E. (2014) A novel ribosomopathy caused by dysfunction of RPL10 disrupts neurodevelopment and causes X-linked microcephaly in humans. *Genetics*, **198**, 723–733.
75. Perucho,L., Artero-Castro,A., Guerrero,S., Ramón Y Cajal,S., Lleonart,M.E. and Wang,Z.-Q. (2014) RPLP1, a crucial ribosomal protein for embryonic development of the nervous system. *PLoS One*, **9**, e99956.
76. Valenti,D., de Bari,L., De Filippis,B., Henrion-Caude,A. and Vacca,R.A. (2014) Mitochondrial dysfunction as a central actor in intellectual disability-related diseases: an overview of Down syndrome, autism, Fragile X and Rett syndrome. *Neurosci. Biobehav. Rev.*, **46**, 202–217.
77. Rogers,M.F., Marshall,O.J. and Secombe,J. (2023) KDM5-mediated activation of genes required for mitochondrial biology is necessary for viability in *Drosophila*. *Development*, **150**, dev202024.
78. Cui,H., Kong,Y. and Zhang,H. (2012) Oxidative stress, mitochondrial dysfunction, and aging. *J Signal Transduct*, **2012**, 646354.
79. Kataria,A. and Tyagi,S. (2023) Domain architecture and protein-protein interactions regulate KDM5A recruitment to the chromatin. *Epigenetics*, **18**, 2268813.

Received: November 9, 2023. **Revised:** March 20, 2024. **Editorial Decision:** March 24, 2024. **Accepted:** March 31, 2024